Title: Dissociation of attentional state and behavioral outcome using local field potentials

Authors: Surya S Prakash[1], J Patrick Mayo[2], Supratim Ray[1*]

Affiliations:

[1]Centre for Neuroscience, Indian Institute of Science, Bangalore, India, 560012.

[2]Department of Ophthalmology, University of Pittsburgh, Pittsburgh, Pennsylvania, USA

***Corresponding Author:** Supratim Ray

Address: Centre for Neuroscience, Indian Institute of Science, old TIFR building, Bangalore, India, 560012.

Telephone: +91 80 22933437 Email: sray@iisc.ac.in

Keywords: visual attention, behavioral outcome, local field potential, alpha, gamma, high-gamma, pairwise phase consistency

Author contributions: J.P.M. collected the data; S.S.P., J.P.M. and S.R. conceived the idea of research; S.S.P. and S.R. analyzed the data; S.S.P., J.P.M and S.R. wrote the paper.

Conflict of interest: The authors declare no competing financial interests.

Acknowledgements: SR was supported by Wellcome Trust/DBT India Alliance (Senior fellowship IA/S/18/2/504003) and a grant from Pratiksha Trust. JPM was supported by NIH Fellowship F32EY02259, NIH CORE Grant P30 EY08098 to the Department of Ophthalmology, the Eye and Ear Foundation of Pittsburgh, and from an unrestricted grant from Research to Prevent Blindness, New York, NY. We thank Dr. John Maunsell for his help in experimental design and data collection.

Abstract

Behavioral outcome (i.e., whether a target is detected or missed) depends on attentional state and potentially other factors related to decision-making, which could in turn modulate the power and phase of neuronal oscillations. Here we investigated whether attentional state (i.e., whether attention is inside or outside the receptive fields of neurons) and behavioral outcome are distinguishable using the power and phase of local field potential (LFP) recorded from electrode arrays in area V4 of monkeys performing an attentional task under different cuing conditions. Since attention also strongly modulates pairwise measures such as spike count correlation and phase consistency which are typically measured across trials, we developed novel methods to obtain single-trial estimates of these measures. Surprisingly, while attentional location was best discriminated using gamma and high-gamma power, behavioral outcome was best discriminated by alpha power and steady-state visually evoked potential. Power outperformed absolute phase, although single-trial gamma phase consistency provided good attentional discriminability. Our results provide a clear dissociation between the neural mechanisms that regulate attentional focus and those that govern behavioral outcome.

Introduction

Attention facilitates behavior by selectively processing relevant sensory information (Carrasco, 2011). In addition to improving behavioral performance, attention also modulates different neuronal signals like spikes (McAdams and Maunsell, 1999; Motter, 1993) and power of local field potential (LFP) oscillations in various frequency bands (Fries et al., 2001; Khayat et al., 2010; Prakash et al., 2021). The power in different frequency bands have often been used to decode the focus of attention (De Sousa et al., 2021; Esghaei and Daliri, 2014; Prakash et al., 2021; Tremblay et al., 2015). For example, we recently found that high-frequency LFP oscillations (>30 Hz) decode attention better than or on par with spikes when multiple electrodes are used (Prakash et al., 2021). This result contrasts with sensory (Kanth and Ray, 2020) and motor decoding (Hwang and Andersen, 2013) where multichannel spikes outperform multichannel LFP. To account for these differences in the mechanisms of cognitive vs sensorimotor processing, we proposed that the elevated performance of high-frequency LFPs is due to comparable spatial spreads of LFP and biophysical circuits that underlie attention (Prakash et al., 2022).

Our previous study (Prakash et al., 2021) probed one aspect of behavior, which is the attentional state of the animal. Since there is no objective measure of where the monkey's attention was at a particular moment, the decoding may have been more related to which side the attentional cue was given. Specifically, the decoding was between conventional cue-in (cue inside the receptive field (RF) of neurons being recorded) and cue-out conditions, although we used the terms attention-in and attention-out to be consistent with previous literature (Fries et al., 2001; Khayat et al., 2010). Another relevant decoding variable that has been extensively studied is the behavioral outcome (hit versus miss). Here, many studies have reported that the phase of low-frequency oscillations are highly informative (Busch and VanRullen, 2010; Harris et al., 2018). However, whether LFP features can be used to decode

the behavioral outcome as well as spikes is not known. This evaluation is important for designing functional brain-computer interfaces and for potentially revealing the neural basis of attention and decision making.

LFP phase consistency has been hypothesized to play a particularly important role in effective communication between neuronal ensembles and has been shown to be modulated by attention (Bosman et al., 2012; Fries, 2015). For example, attention enhances the spike-LFP and LFP-LFP phase coherence in the gamma band in macaque visual area V4 (Buffalo et al., 2011; Fries et al., 2001; Prakash et al., 2021). Likewise, behavioral performance measured using reaction time is also shown to vary with the absolute LFP phase (Ni et al., 2016), spike-LFP phase coherence (Womelsdorf et al., 2006) and inter-areal LFP-LFP phase consistency (Rohenkohl et al., 2018) in the gamma band. Collectively, a substantial body of work suggests that phase relationship between neuronal population is systematically modulated by both attention and behavioral performance.

Because phase consistency measures are typically calculated across trials (but see (Spyropoulos et al., 2023), they may fail to capture the well-established trial-by-trial changes in attentional fluctuations and behavioral performance that we seek to understand (Cohen and Maunsell, 2011, 2010; Ghosh and Maunsell, 2021; Roy et al., 2021) Thus, existing methods for calculating phase consistency may provide only a coarse estimate of the underlying dynamics of attention or behavioral state. Notably, this shortcoming is not limited to LFP measures. Conventional measures of spike count correlation between two neurons—which have been shown to reduce with attention (Cohen and Maunsell, 2009; Mayo and Maunsell, 2016; Mitchell et al., 2009)—suffer from the same limitation. To address these issues, we developed novel methods to compute pairwise metrics such as spike count correlation, LFP power correlation, and field-field coherence for single trials, and tested the ability of spikes,

LFP power, LFP phase, and these pairwise metrics in visual area V4 in decoding attention and behavioral outcome of two rhesus macaques performing a change detection task.

Results

We recorded spike activity and local field potentials (LFPs) using microelectrode arrays implanted in both hemispheres of area V4 in two monkeys. Monkeys performed an attention task in which two Gabor stimuli that counterphased at 10 Hz were presented on a screen and the monkeys were cued to either attend to one or both stimulus locations (see Methods for details) in separate blocks of trials. In trials where one location was cued, the target (change in the orientation of the Gabor) occurred on the cued side in 80% of trials (validly cued) and on the uncued side in 20% of trials (invalidly cued). In addition, there were trials where both sides were simultaneously cued (neutral cue) and the target could appear on either side with equal probability.

Trials were categorized into different conditions based on cue/target locations (attend/target inside or outside the RF), cue types (valid, neutral, or invalid), and behavioral outcomes (hit or miss). Invalidly cued trials were not analyzed due to insufficient number of trials (see 'Data analysis' section in Methods for more details). Since the monkeys were cued to attend to both locations in neutral blocks, we categorized those trials based on the target location instead of cue location. This resulted in the following eight conditions (four each for valid and neutral cueing): Attend-In Valid Hit (AIVH), Attend-Out Valid Hit (AOVH), Attend-In Valid Miss (AIVM), Attend-Out Valid Miss (AOVM), Target-In Neutral Hit (TINH), Target-Out Neutral Hit (TONH), Target-In Neutral Miss (TINM), Target-Out Neutral Miss (TONM).

Attentional and Behavioral Discriminability using firing rate and LFP power

Figure 1A shows the average peri-stimulus time histogram (PSTH) of 677 electrodes across 22 sessions for the four validly cued conditions during 500 – 0 ms before the target onset.

Neurons fired at both the positive and negative phases of the counterphasing stimulus to produce a strong oscillatory signal at 20 Hz (De Valois et al., 1982). The average firing rates over this 500 ms interval are shown in the inset. The firing rate was higher when the monkeys attended and detected (hit) the target presented inside the RF (AIVH condition; blue) than when they attended and detected the target outside the RF (AOVH condition; red). This recapitulates the classic effect of visual attention on the firing rates of cortical neurons, whereby the responses to attended stimuli in the RF are enhanced, on average, relative to unattended stimuli (McAdams and Maunsell, 1999). The conditions when the monkeys missed the target are expected to produce a response that is intermediate between these two hit conditions since attention is expected to be on the uncued side leading to the miss. We indeed observed this effect when the monkeys attended and missed the target presented outside the RF (AOVM; magenta), but not inside (AIVM; cyan), for which the response was comparable to AIVH condition (the reason for this discrepancy is due to a mismatch between the target onset times for hits versus misses, as explained below).

Surprisingly, event related potential (ERP), obtained by averaging the LFP traces for different conditions, showed a more pronounced difference between the hit and miss conditions than firing rates (again, the reason is explained below). We observed a prominent drift in ERP for miss condition of both the attention conditions (Fig.1B, magenta and cyan). This drift increased the power in low-frequency range (<14 Hz) in the power spectral density (PSD) for both the miss conditions, which can be observed in Fig. 1C where change in power of each condition from AOVH condition is shown. The effect of attention on the PSD is shown by the blue trace in Fig 1C, which shows the change in power when attention is inside versus outside the RF (AIVH versus AOVH). Attention suppressed the power in lower frequencies and increased power in the gamma range (>30 Hz) as well as the steady-state-visually-evoked-potential (SSVEP) frequency of 20 Hz (Prakash et al., 2021). The effect of behavioral

outcome (hit versus miss) was observed when attention was outside the RF and the monkey missed the target (magenta trace; AOVM versus AOVH), or by comparing the corresponding conditions for the Attend-In condition (i.e., blue versus cyan traces; AIVH versus AIVM). Here, the miss conditions had much higher power at low frequencies as compared to the hit conditions. Overall, low frequencies captured differences in activity related to behavioral outcome, while frequencies closer to gamma distinguished attentional state.

To better dissociate the effects of attentional location and behavioral outcome and examine how the effect of one is influenced by the other, we compared the PSDs separately by taking the difference between the attention conditions (attend-in versus attend-out) for the two behavioral outcomes: hit (Fig 1D, green trace; same as the blue trace in Fig 1C) and miss (Figure 1D, yellow trace; cyan minus magenta traces in Fig 1C). Attention-related suppression of low-frequency power (<30 Hz) and enhancement of the high-frequency power (>30Hz) was also observed for the miss condition, albeit the effect was weaker than the hit condition (compare green versus yellow traces in Fig.1D). Similarly, for behavioral effects we took the difference between the behavioral outcomes (hit – miss) for the two attention conditions: attend-in (blue trace in Fig 1E; blue minus cyan traces in Figure 1C) and attend-out (red trace in Fig 1E; same as the negative of the magenta trace in Fig 1C). For the behavioral comparison (Fig. 1E), the power in the low-frequency range showed a huge negative difference for both attend-in and attend-out cases, whereas high-frequency power showed only minor differences.

Since one of the aims of the study was to compare the ability of different neural measures (such as spiking activity, LFP power, and LFP phase) to discriminate attentional conditions and behavioral outcome, we converted the LFP power and spike responses to d-prime values to compare the discriminability across neural measures (Fig 1F and 1G; see Methods for details). Attention discriminability using firing rates (indicated by dashed lines in 1F) was

higher for hit condition (green dotted line) than miss (yellow dotted line), reflecting larger separation in the means for the hits compared to miss cases (as in Fig. 1A inset). Attention discriminability with LFP power was highest in the gamma band (40 -80 Hz), was comparable to that of firing rate, and decreased slowly at higher frequencies (solid green and yellow traces in 1F; note that discriminability increases when power is averaged across frequencies, as shown below). Lower frequencies (<30 Hz) had negative d-prime (i.e., attend-in condition had lower power than attend-out as shown in Fig. 1D), but the magnitude of the discriminability was lower than that of firing rate. On the other hand, very low frequency (<14 Hz) power was best suited for discriminating the behavior (Fig. 1G) since it had the highest magnitude of discriminability, reflecting the changes in power observed in Figure 1E.

We further investigated the prominent drift and the inconsistency in firing rates observed for miss conditions and found that they could be largely explained based on differences in target onset times for hits versus miss conditions: monkeys tended to miss the targets that appeared earlier after stimulus onset than later (Fig 1H). Stimulus onset produced a transient elevation in firing rate and a dip in the ERP which reached a steady state value over several hundred milliseconds (see Figure 1A, B of Prakash et al., 2021). Thus, because our analysis window was 500 to 0 ms before the target onset (which could appear between 500-5500 ms of stimulus onset), we may have captured the transient activity for the trials in which the target appeared between 500 to 750 ms after the stimulus onset. Hence, the differences observed between hit and miss trials may have been indirectly influenced by artifacts of task performance timing.

To address this concern, we analyzed the data after matching the target onset time distributions of the hit and miss trials of the respective attention conditions (see Methods for details). Figure 1I-1O show the same analyses as 1A-1G but after matching target onset time distribution averaged over 643 electrodes for valid cue condition across 21 sessions. The

firing rate for the AIVM condition now became less than AIVH, as expected since attention is expected to be away from the RF when the monkey missed the target (cyan and blue dots in inset in Figure 1I). The strong drift observed earlier mainly in the miss conditions (Fig. 1B) was now comparable to that of the hit conditions (Fig. 1J).

Using this target onset matched approach, the difference in power in the very low-frequency range was drastically reduced for the missed condition relative to the hit condition (Fig 1K and Fig 1M) compared to that in the non-matched case (Fig 1C and 1E). For example, the change in 4Hz power of attend-in valid miss (AIVM) relative to attend-in valid hit (AIVH) reduced by more than three-fold in distribution matched (0.75 dB) compared to non-matched case (2.4 dB) (Fig 1M and 1E). These results highlight that the pre-target low frequency power can spuriously dominate and lead to an overestimation of its behavioral decoding performance if the differences in the distribution of target onset times between the conditions are not accounted for. For remaining analyses, we therefore only use trials after matching target-onset time distributions.

After target-onset distribution matching, two salient results remained: (1) d-prime values for LFP power for attentional discriminability (Attend-In versus out; Figure 1N) for hit condition (green trace) were highest in the gamma band, where it was comparable to d-prime of firing rate, and decreased in the high-gamma range. It was negative at low frequencies, although the magnitude was less than the gamma range. Similar trends were observed in the miss condition (yellow trace), although magnitudes were lower. (2) For behavioral discriminability (Fig 1O) for attend-in condition (blue solid trace), d-prime values were negative at low frequencies, became positive at SSVEP frequency and in high-gamma range, comparable to the discriminability using firing rate (blue dashed line). The highest d-prime was observed for the SSVEP frequency. The effect flipped for the attend-out condition in the high-gamma range (red solid trace).

We previously showed that the single electrode LFP power in the gamma (42-78 Hz) and high-gamma (122-198 Hz) band performed better than firing rate in decoding attend-in valid hit vs. attend-out valid hit (Prakash et al., 2021). However, in our present analysis, the power in the gamma and high gamma ranges did not perform better than firing rate in discriminating the attention condition (Fig. 1N; green trace). This discrepancy is due to the variability in the spectral estimator at individual frequency bins (Jarvis and Mitra, 2001), which decreases d-prime values as observed here. However, spectral variability is uncorrelated across frequencies and therefore can be reduced by summing or averaging the power over the frequencies of interest, which can improve the decoding performance (Prakash et al., 2021). We illustrate this fact by performing similar averaging by smoothening over a frequency window using Multitaper method. The extent of frequency smoothening is controlled by the time-bandwidth product (TW) which determines the number of tapers (K) to use (K = 2TW-1) for maximal spectral concentration. Increasing TW increases the frequency window over which the power is smoothed. As expected, as we increased TW, the attentional d-prime in the gamma and high-gamma band increased and exceeded the d-prime of firing rate as in our earlier study (Fig. 1P). Note that the enhanced discriminability at SSVEP was eliminated by this smoothing because the nearby frequencies did not show this discriminability. Thus, frequency smoothing improves the discriminability when the neighboring frequencies perform comparably well.

The neutral cueing condition showed similar results (supplementary fig.1; compare A-G versus I-O). As in the valid condition, firing rates were higher when target appeared inside the RF than when it appeared outside (supplementary fig. 1A and 1I inset) and the drift in ERP observed mainly in miss conditions (supplementary fig. 1B) became comparable to hits when target onset distributions were matched (supplementary fig. 1J). However, there were some important differences as well. Firing rates were different for hits versus misses when

target was inside the RF (blue and cyan dots in panel supplementary fig. 1I that correspond to TINH versus TINM conditions), but not when the target was outside the RF (TONH versus TONM). This trend was also reflected in the LFP power, with large discriminability in behavior the gamma range (which was further comparable to the firing rate discriminability) when target was in the RF (blue trace in supplementary fig. 1O) but not when outside (red trace in supplementary fig. 1O). The discriminability between target-in and target-out conditions for hit trials was highest in the gamma range and was comparable to the firing rate (green trace in supplementary fig. 1N) and the traces were essentially inverted for the miss condition for both firing rate and LFP power (yellow traces supplementary fig. 1N). Unlike the valid condition, frequency smoothening did not improve discriminability beyond firing rates (supplementary fig. 1P). Overall, the behavioral discriminability pattern of neutral cue was similar to the attentional discriminability of the valid condition (in other words, effect observed in Figure 1N was similar to supplementary fig. 1O, while Figure 1O was similar to supplementary Fig. 1N).

Discrimination of attentional state and behavioral outcome using phase

EEG studies have shown that phases at frequency bands such as alpha (8-12 Hz) are modulated by attention and are informative about behavioral performance (Busch et al., 2009; Thut et al., 2006). We therefore examined the ability of LFP phase to discriminate the attentional and behavioral states. If the LFP phases at which monkeys detect the target are consistently different from the phases at which they miss, the difference should be reflected in the ERPs, which we did not observe (Figure 1J; although note that the presence of strong SSVEP may have affected the endogenous alpha rhythm). Because phase is a circular variable, we used the sine component of the phase vector to make it linear (like firing rate and

LFP power) in order to calculate d-prime. This transformation should not affect our results since we are interested in the differences between conditions rather than their absolute values. For valid trials, the phase values were only consistent at the SSVEP frequencies (Fig 2A), but we did not find a consistent difference across conditions at any frequency, resulting in low attentional and behavioral discriminability compared to the firing rate (Fig.2B and 2C). Similar results were obtained when the cosine component was used instead of the sine component (data not shown).

We previously showed that pairwise phase consistency (PPC) across pairs of electrodes, which reflects the consistency of the phase difference between electrodes across trials, varied with attentional condition (see Figure 2 of Prakash et al., 2021). We next tested whether absolute phase of a single electrode also showed any consistency across trials. For this analysis, we computed the PPC, which is an unbiased estimator of the square of the coherence (Vinck et al., 2010), but replaced the phase difference between a pair of electrodes with the absolute phase of one electrode for each trial. This single-electrode PPC is expected to be high if the absolute phase is consistent across trials. However, PPC was high only at the SSVEP frequency (the peak is seen at 24 Hz instead of 20 due to smoothening effect of Multitaper) and its harmonics (Fig. 2D). No consistent trends were observed when we compared across conditions (Fig. 2E and 2F). Note that since PPC is computed across trials, it is not a single-trial measure and therefore we cannot obtain d-prime values like above. In summary, the absolute phase of the LFP was much less informative about the attentional location or behavioral state than firing rates, and no difference in the consistency of the phase across trials was observed across conditions. Similar results were obtained for the neutral cue (Supplementary fig. 2).

Effect of attention and behavioral outcome on pairwise measures

Conventional measures based on pairs of electrodes, such as correlation and phase consistency, are computed across trials. Before exploring single-trial estimates of such measures, which are required to estimate discriminability, we evaluated the effects of attention and behavior the traditional way by computing these measures across trials. Consistent with previous studies (Cohen and Maunsell, 2009; Mayo and Maunsell, 2016; Mitchell et al., 2009), attention reduced correlations in firing rate across pairs of electrodes (AOVH versus AIVH; Fig. 2G). The correlation for missed conditions were intermediate to the hit condition (AOVM and AIVM; Fig 2G), consistent with the changes in Figure 1I inset. Correlations between LFP power recorded from two electrodes increased with attention at SSVEP frequency (20 Hz) and its harmonic but reduced for frequencies higher than 50 Hz for valid hit condition (Fig.2H; green trace). Such modulations were not observed when the animals missed the trials (yellow trace in Fig 2H). Differences between behavioral outcomes (hit versus miss; Fig 2I) were small in the high-gamma range, mirroring the small changes observed in firing rate correlations as well. Interestingly, lower frequencies including the SSVEP frequency showed larger differences for Attend-out condition (red trace in Fig 2I) which is similar to the strong effect of behavioral differences on SSVEP power observed earlier (Fig 1O). Overall, these results are consistent with previous studies that showed a reduction in spike count correlation (Cohen and Maunsell, 2009; Mitchell et al., 2009) and LFP power correlation except at SSVEP (Prakash et al., 2021).

Next, we analyzed the PPC between the LFP signals from pairs of electrodes (Fig. 2J-L). PPC increased for valid condition when attention was cued into the RF over a broad range of frequencies between 36 Hz to 106 Hz (Fig. 2K; green trace), although we did not observe much difference beyond 120 Hz even though LFP power was elevated in that range (compare with the green trace in Fig. 1L). Reasons for this difference between high-frequency power

and PPC are discussed elsewhere (Ray, 2022). Interestingly, PPC was more sensitive to attentional differences (Fig. 2K) than behavioral differences (Fig. 2L).

For neutral condition (supplementary fig.2), the effect of target location (supplementary fig. 2H and supplementary fig. 2K) was somewhat similar to behavioral effect (Fig. 2I and Fig. 2L) of the valid condition and the behavioral effect (supplementary fig. 2I and supplementary fig. 2L) was similar to attentional effect (Fig. 2H and Fig. 2K) of the valid condition, as observed previously with LFP power (Supplementary fig. 1N was similar to Fig. 1O with the two traces flipped horizontally, while supplementary fig. 1O was similar to Fig. 1N with one trace showing salient effect and the other one close to zero).

Discrimination of attentional state and behavioral outcome using pairwise measures

Modulation of pairwise measures by attentional state and behavioral outcome motivated us to develop methods to obtain the same measures in single trials, which could then be used to obtain discriminability values (d-prime) like the power and phase measures we used earlier. We devised two independent methods to estimate correlation and phase consistency within a single trial. In the first method, we divided the spiking and LFP signal of a single trial into ten non-overlapping bins of 50 ms each and computed firing rate, LFP power, and phase in each bin. We then calculated the correlation and LFP-LFP phase consistency between electrode pairs across bins (Fig.3, left panel). In the second approach we used the Multitaper method where a single trial LFP signal was multiplied by nine orthogonal Slepian tapers to obtain nine independent estimates of LFP power and phase (Fig. 3, right panel) and computed their correlation and phase consistency (see Methods for more details). The first method is more direct because power and LFP values are obtained from non-overlapping segments of data, although the frequency resolution (reciprocal of the analysis duration in seconds) becomes 20

Hz. The second method uses the same length of data (500 ms) to get several estimates of power and phase (which are independent because the tapers are orthogonal) and therefore has a frequency resolution of 2 Hz.

Firing rate correlations were reduced with attention for hit trials even when computed over a single trial (Fig. 4A, dashed green line), but not reduced in miss trials (Fig. 4A, dashed yellow line), consistent with the across-trial correlation measures (Fig. 2H). Even the single-trial LFP power correlation computed using the binning method showed similar effects as that of the traditional correlation measure (compare solid green and yellow traces in Fig. 4A with the same traces in Figure 2H). Because these were single-trial measures, we could now calculate and compare the discriminability by calculating d-prime values in the same way as before (Figure 4B). LFP correlations in the high-gamma range could distinguish the attention conditions slightly better than firing rate correlation when the targets were correctly detected (Fig. 4B; green trace), although these d-prime values were considerably lower than the ones obtained using firing rate/LFP power (compare with similar traces in 1N). Similar trends were obtained for behavioral comparison: (1) single trial correlations (Fig 4C) mirrored the results obtained using across-trial correlations (Fig. 2I), (2) magnitude of discriminability (Fig 4D) was higher in the high-gamma range where it was comparable to firing rate correlations for the attend-in condition (blue traces in Fig 4D), and (3) for the attend-out condition the low-gamma frequencies were more discriminable (red trace in Fig 4D) than firing rate for that condition. In summary, we found that our single trial estimates of correlation showed modulations similar to the traditional trial-wise correlation and the discriminability of high-gamma and firing rate correlations were comparable.

Results of single-trial bin-wise PPC (Fig 4E and 4G) also showed similar trends as that of conventional trialwise PPC (Fig. 2K and 2L). However, the magnitude of d-prime values was considerably higher (4F and 4H) compared to that of correlations in firing rate/power,

suggesting that single trial PPC, especially in the gamma range, was a useful measure to discriminate attention or the behavioral outcome.

Although bin-wise PPC reflected most of the trends seen in trialwise PPC, the binning method was inherently limited in its frequency resolution. To overcome this limitation, we used the Multitaper method and computed correlation and PPC across tapers (Method 2 in Fig 3). The binning and Multitaper methods produced similar results, validating our approaches. For correlations (Fig 4I-L), while the trends were generally similar to the bin-wise approach (compare with Figure 4A-D), we found two important differences. First, while the high-gamma band beyond 100 Hz essentially reflected the trends observed in firing rates for the bin-wise method (e.g., Fig 4A), the Multitaper method produced negligible correlation differences above 100 Hz (e.g., Fig 4I). On the other hand, the difference in LFP correlations between the conditions improved remarkably in the gamma band and below (<60 Hz) and hence the discriminability index increased threefold compared to the binning method (compare 4B and 4D with 4J and 4L; note the difference in scales). In contrast, the PPC measure (Fig 4M-P) remained comparable across both methods (Fig 4E-H).

Among the electrode pair measures, PPC in the low to mid frequency range was the most useful measure to discriminate attention and behavior. For the neutral conditions (Supplementary fig. 3), the trends were similar to their across-trial counterparts (Supplementary fig. 2) and reflected the same results as observed for valid trials. Finally, because our analyses in Fig 1P demonstrated that discriminability differs as a function of smoothening over frequency ranges, we computed all of the LFP measures according to frequency bands of alpha (8-12 Hz), SSVEP (18-22 Hz), gamma (40-80 Hz), high-gamma (120-200 Hz) and summarize our results in Figure 5. Same results for the neutral condition are shown in Supplementary Figure 4.

Our key findings are summarized as follows: 1) LFP power in the high-gamma and gamma bands were best suited for discriminating “attend-in” vs. “attend-out” attentional state (d-prime values of 0.32 ± 0.01 and 0.3 ± 0.01; Fig.5A). Firing rate was the next most informative measure (d-prime of 0.22 ± 0.01; Fig.5A), but discriminability using gamma was significantly greater than that of firing rate ($p = 7.5\times10^{-18}$; Wilcoxon rank sum test). Alpha power also had strong discriminability (d-prime of -0.14 ± 0.01), although the magnitude was significantly less than firing rate ($p = 7\times10^{-18}$; Wilcoxon rank sum test). 2) While gamma, high-gamma, and spiking activity could all be reliably used to discriminate attentional state, alpha power, SSVEP power, and SSVEP phase were the most informative measures for discriminating behavioral outcome (Fig. 5B). In general, firing rates and high-frequency LFP (gamma and high-gamma) were not very useful to discriminate behavior. 3) Among the phase-based measures, single trial PPC in the gamma band was the most informative of the attentional state, especially when calculated using the Multitaper method (d-prime of 0.23 ± 0.004; purple bar in Fig 5A), on par with the firing rate ($p = 0.07$; Wilcoxon rank sum test). 4) The performance of the neural measures in the discriminating behavioral outcome for neutral condition was similar to the discrimination of attentional conditions for valid condition (Supplementary fig. 4B).

Discussion

We studied the effect of attentional (cue inside vs outside RF) location and behavioral outcome (hit vs miss) on distinct frequency bands of the LFP. Our analyses illustrated potential issues caused by visual transients that can differentially affect measures of behavioral outcome, which could be corrected by matching the target onset distributions for different conditions. While high-frequency LFP power in the gamma (42-78 Hz) and high-gamma (122-198 Hz) band decoded the attentional state best, low frequency power in the alpha (8-12 Hz) and SSVEP (18-22 Hz) range also decoded the behavior well. We also developed novel single-trial estimates of correlation and pairwise phase consistency (PPC) which showed similar attention and behavioral modulations as their trial-wise counterparts. Although these metrics did not produce the best decoding performance in our dataset, but they will likely be useful for future investigations of the dynamics of attention. Phase-based measures performed poorly compared to power-based measures. Nonetheless, among the phase-based measures, taper-wise PPC in the gamma band was the best, performing on par with the firing rate in decoding attention.

Comparison with previous studies

LFP high-gamma power has been shown to reflect the average firing rate of the neuronal population around the microelectrode tip (Ray et al., 2008; Ray and Maunsell, 2011). Unlike LFP, the increase in high-gamma power in electrocorticogram (ECoG) – a signal which integrates over a larger population than LFP – cannot be accounted solely by increases in firing rate and has been hypothesized to reflect more synchronous or correlated activity in the neural population (Ray et al., 2008). Interestingly, we found that attentional discriminability of LFP high-gamma power was higher than that of firing rate which suggests that, like ECoG,

high-gamma power of LFP could also partially reflect firing rate correlations and synchrony (in addition to the average firing rate) which also get modulated with attention (Cohen and Maunsell, 2009). In addition, improved performance of higher LFP frequencies could simply be due to optimal averaging of responses in the LFP signal over the spatial scale over which attention operates, as argued previously (Prakash et al., 2022).

Our results are consistent with the findings of human EEG studies (Busch et al., 2009; Hanslmayr et al., 2007; Thut et al., 2006) which showed that alpha power was lower when subjects detected a visual target than when they missed it, although we note that the endogenous alpha rhythm in our study could be compromised because of the strong 10 Hz counterphasing stimulus. However, care should be taken to match the distribution of target onset times for hit and miss trials while analyzing the data in the pre-target period to avoid the effect of stimulus onset related transients that can artificially inflate the behavioral effects on low frequency power, especially in a change detection task which is often used in attention studies.

We found the performance of phase-based measures underwhelming given many studies have shown the importance of phase in attention and behavioral performance (Busch and VanRullen, 2010; Fiebelkorn et al., 2018; Rohenkohl et al., 2018). For example, attention improved the consistency of gamma-band phase relations between two neuronal groups, which is thought to be crucial for the effective relay of information (Fries et al., 2001). Attention is also suggested to operate in a rhythmic manner which is mediated by the phase of alpha and theta band (Busch and VanRullen, 2010; Fiebelkorn et al., 2018; Landau and Fries, 2012), although a recent study has questioned these results (Brookshire, 2022). Previous LFP studies which used reaction time as the behavioral readout have shown that absolute phase (Ni et al., 2016) and phase coherency (Womelsdorf et al., 2006) in the gamma band to be predictive of behavior. Despite these mechanistic implications of phase on

attention, we did not find any effect of absolute phase. Even with pairwise measures, only gamma-band PPC managed to perform well in discriminating attentional state, although not as well as power-based measures. Interestingly, the attentional discriminability of gamma-band PPC was comparable to that of firing rate, contrary to a recent finding where V4 firing rate decoded attention better than inter-areal gamma-band PPC between V1 and V4 (Spyropoulos et al., 2023). Furthermore, several EEG studies (Busch and VanRullen, 2010; Harris et al., 2018), showed that the detection performance at the cued location systematically depended on the phase of the alpha-band, their performance in discriminating the behavioral outcome was marginal. The performance of SSVEP phase measures, on the other hand, was comparable to that of its power. Our results of LFP power-based measure performing better than phase-based measures are consistent with a similar finding in epidural ECoG recordings in macaque visual area V1 and V4 (Rotermund et al., 2013).

Shared and distinct effects of attention and behavior on LFP

Although subjects are better at detecting the target when it appears at the cued location, they occasionally miss the target. If this is due to the misallocation of attention, the modulation of neural activity by attention (attend-in vs attend-out) and behavioral outcome (hit vs miss) should be similar, which was not the case. One reason could be that in a missed trial, the overall attentional (or arousal) level could be low (rather than focused on the incorrect side), which would further be reflected in the power of low-frequency rhythms such as alpha (Hong et al., 2014; Johnston et al., 2022; van Kempen et al., 2019). Further, a behavioral report involves a decision variable, and hence relates to different aspects such as bias or criterion, as compared to changes in sensitivity (Banerjee et al., 2019; Luo and Maunsell, 2019; Sridharan et al., 2014). Some studies have suggested that bias could be reflected in alpha power (Iemi et

al., 2017; Limbach and Corballis, 2016; Samaha et al., 2020) but see (Podvalny et al., 2021; Zhou et al., 2021), potentially leading to better discriminability of behavioral outcome using alpha power. Saccade preparation is another factor which can modulate the low-frequency oscillations in V4 (Steinmetz and Moore, 2014) that might contribute to better behavioral discriminability. However, a recent study which used the same experimental data found no difference in the microsaccade direction – a potential indicator of saccade preparation (Hafed and Krauzlis, 2012) - between hits and miss trials (Willett and Mayo, 2023).

Our results also relate to potential roles of fast (gamma) and slow (alpha/beta) oscillations in mediating feedforward and feedback communication across brain areas, as proposed by some studies (Bastos et al., 2015; van Kerkoerle et al., 2014). This notion implies that attentional modulation somehow affects the feedforward pathway while behavioral outcome (target detection) affects feedback, which is unlikely for several reasons. First, attention is shown to enhance gamma-band causal influence (Granger causality) in both feedforward and feedback directions between area V4 and V1 and within V4 (Ferro et al., 2021). Second, attention signals are shown to originate from higher areas like frontal eye field (FEF) which sends a long-range feedback connections to V4 (Gregoriou et al., 2009). On the other hand, the behavioral outcome effects could be mediated through the feedback pathway because an enhancement of alpha band activity was observed in lateral intraparietal area (LIP) when the perceptual sensitivity was low which can lead to a miss and a boost in the beta band activity in FEF when the perceptual sensitivity was high which can lead to a hit (Fiebelkorn et al., 2018). The inter-areal coherence usually increases in the frequency bands which have higher power (Schneider et al., 2021) and consequently the behavioral outcome information can propagate through the low-frequency mediated feedback signal to lower areas like V4. Therefore, our results show that modulation of high or low frequency oscillations might not always result from the exclusive engagement of feedforward or feedback pathways

respectively, but instead can arise from both feedforward and feedback, at least for attentional effects.

Decoding performance in the neutral condition

There were similarities as well as stark differences in discriminability of attention and behavioral outcomes in neutral condition. Like in valid condition, LFP power was better at decoding than phase measures. However, high-frequency oscillations were better in decoding behavioral outcome than attention location, in contrast to valid condition. The difference in the discriminability pattern could be due to the differences in the strategies employed in the two cue conditions. In the neutral condition, subjects likely had to divide their attention or switch between the two locations since the target was equally likely to appear at either location. The similarity between the decoding pattern of behavioral outcome (Hit vs Miss) in neutral condition and attention (attend-in vs attend-out) in valid condition suggests that the focus of attention was outside the receptive field whenever the subjects missed the target that appeared inside the receptive field, since the target was also equally likely to occur on either side, making it similar to the attend-in and attend-out of the valid condition. This explanation holds only if the subjects were switching between the two locations. However, we do not know the exact strategy the subjects used during neutral cue; future experiments that control for the strategies employed by the subject may help resolve the similarities observed between the decoding patterns of different states of the valid and neutral conditions.

Overall, the differential ability of distinct LFP bands in discriminating attention and behavioral states not only highlights the usefulness of LFP in segregating the information

related to different cognitive and behavioral state but also provides insights into their underlying mechanisms.

Methods

Electrophysiological recordings

Data and experimental procedures used in this study are described in our previous studies (Mayo and Maunsell, 2016; Prakash et al., 2021). We outline the details briefly here. All the animal procedures were approved by the Institutional Animal Care and Use Committee of Harvard Medical School. Two adult male rhesus monkeys (*Macaca mulatta*) were surgically implanted with a titanium headpost and scleral eye coil before training on the task. After training, each monkey was implanted with two 6 × 8 (48) microelectrode Utah arrays (Blackrock Microsystems), one in visual area V4 of each hemisphere. Electrodes were 1 mm long and 400 µm apart. The impedances of the electrodes were in the range of 0.2 – 1MΩ at 1 KHz.

The raw signals from 96 channels were recorded using a 128-channel Cerebus Neural Signal Processor (Blackrock Microsystems). Single and multi-unit spiking activity were obtained by filtering the raw signal between 250 Hz (4th order digital Butterworth filter) and 7.5 kHz (3rd order analog Butterworth filter) and subsequently subjected to a voltage amplitude threshold and sorted offline using spike sorting software (Plexon). LFP signal was obtained by filtering the raw signal between 0.3 Hz (1st order analog Butterworth filter) and 2.5 kHz (4th order digital Butterworth filter), sampled at 2 kHz and digitized at 16-bit resolution. The possible aliasing caused by inadvertently setting the low pass LFP filter cutoff at a frequency that was higher than the sampling frequency had negligible effect on the LFP (Prakash et al., 2021).

Behavioral task

Monkeys were trained to perform an orientation change detection task. A trial began with the appearance of a small fixation spot at the center of the monitor, and the monkeys held their gaze within a 1.8º square window centered on the fixation spot throughout the trial. Two full

contrast Gabor stimuli were presented simultaneously and synchronously on a CRT monitor (100 Hz frame rate, 1024 × 768 pixels) over a uniform gray background, positioned 57 cm from the monkeys. Each Gabor was sinusoidally counterphased at 10 Hz and its size, location, spatial frequency, and initial orientation were optimized for a randomly selected recording channel in each hemisphere during each session. At a random time chosen from an exponential distribution (mean: 3000 ms; range: 500 – 5500 ms) when the contrast of both the stimuli were at 0%, one of the stimuli changed its orientation. Monkeys were rewarded for making a saccade to the changed stimulus between 100 and 550 ms after the change. Eye position was sampled at 200 Hz using the scleral eye coil technique.

Monkeys were cued to attend to one (valid-invalid condition) or both stimuli (neutral condition) in blocks of ~50 trials, each beginning with four correct instruction trials in which a small white spot appeared briefly for 50 to 100 ms indicating the location(s) of the change (target). In valid-invalid blocks, the target appeared at the cued location with 80% probability (valid cue) and 20% probability at the uncued location (invalid cue). In neutral blocks, the target appeared at either location with 50% probability. Five percent of the total trials were catch trials in which no change occurred, and monkeys were rewarded for maintaining the fixation throughout the trial. Catch and instruction trials were not included in the analysis. Six different orientation change magnitudes were used for valid and neutral cue conditions and only the second and third smallest orientation change were used to probe attention in the invalid condition in each recording session.

Data analysis

We analyzed the data from 25 sessions of two monkeys (Monkey A: 13 sessions; Monkey W: 12 sessions). We restricted our analysis to trials with either the second or third smallest orientation change in which the behavioral performance was close to 50% to obtain a

comparable number of trials between hit and miss conditions. Note that the magnitude of orientation change can be different for different cue types and locations. In addition, we considered data for a particular cue condition of a given session only if there were more than 10 trials in each of their four conditions. Consequently, 22 out of 25 sessions met the criteria for valid and neutral cue but none for invalid cue. Hence, we only analyzed the data of valid and neutral cue conditions.

Mean matching of target onset time distribution

We matched the target onset time distribution of hit and miss trials of each attention condition to remove the artifactual drift introduced due to the difference in the number of early target onset (<750 ms) trials. We sorted the hit and miss trials separately based on the target onset times (500-5500 ms) and divided them into bins of 250 ms and randomly chose an equal number of trials from both the conditions in each bin. We performed the analysis (Figure 2 onwards) on the mean matched data and computed all the neural measures. The process was repeated 50 times and then averaged across iterations.

Spiking and LFP analysis

We analyzed the spikes and LFP data between 500 to 0 ms before the target (orientation change) onset to obtain the following measures.

Single electrode measures:

Trial-wise measures:

Peristimulus time histogram (PSTH): PSTH was obtained by counting spikes in non-overlapping 10 ms bins for all the trials and converting them into firing rate which were then averaged across trials.

Evoked response potential (ERP): ERP is obtained by trial averaging the LFP signal in the analysis period.

Single-electrode pairwise phase consistency (PPC): Traditionally, PPC quantifies the consistency of phase difference between two signals, like spike and LFP from the same electrode or spike-LFP or LFP-LFP from two different electrodes (Vinck et al., 2010). In single-electrode PPC, we simply used the absolute phase rather than phase difference. We estimated five phase values using the Multitaper method with five Slepian tapers (Jarvis and Mitra, 2001) using Chronux toolbox (Bokil et al., 2010) in MATLAB. Then, we calculated the PPC for the phase estimate of each taper and averaged the PPC values across tapers to obtain the PPC value for each electrode.

Single trial measures:

Power spectral density (PSD): We estimated the power of the LFP signal in 0 to 200 Hz frequency range for each trial with 2 Hz resolution using the Multitaper method with five Slepian tapers.

Phase: Phase was estimated by taking the Fourier transform of the LFP signal. To account for the circular nature of the phase data, we used the sine component of the phase angle as the measure.

Electrode pairwise measure:

Trial wise measure:

Firing rate/ LFP power correlation: Pearson correlation between the firing rates or LFP powers of pairs of electrodes were computed across trials.

LFP-LFP PPC: The phase relationship between the LFP signals of pairs of electrodes was quantified using PPC, an unbiased estimate of square of the phase lock value measuring the

consistency of the phase difference of LFP signals between two electrodes across pairs of trials. We obtained five phase angles at each frequency for each electrode using Multitaper method with five Slepian tapers and then computed the PPC of taper averaged phase difference between two electrodes across pairs of trials.

***Single trial measure*:**

Traditionally, electrode pairwise measures like correlation and PPC are measured across trials. But we needed a single trial measure of these pairwise measures to predict the attention and behavioral state of the monkeys on each trial. Hence, we developed the following two methods to estimate the correlation and phase consistency of a single trial.

1) Binning: We divided spiking and LFP data of 500 ms length into ten non-overlapping segments of 50 ms each. We computed firing rate and LFP power in each segment resulting in ten estimates of firing rate and LFP power with a frequency resolution of 20 Hz. Correlation and phase consistency were computed across these ten estimates.

2) Multitaper: Multiple independent estimates of LFP power and phase for a trial can also be obtained using Multitaper method, where a single trial LFP data is multiplied by several orthogonal tapers and then Fourier transformed to obtain several estimates of power (by squaring the amplitude) and phase (see Fig. 3). We used nine tapers to obtain nine independent estimates of power and phase for a trial and computed correlation and phase consistency across them.

Discriminability using d-prime

We were interested in quantifying the separation in the distributions in the responses for two classes (Attend-In versus Attend-out or Hit versus Miss). Such discriminability is typically quantified using d-prime, which quantifies the difference in the means of the two distributions normalized by their average standard deviation. Here, we used pooled standard

deviation to account for unequal number of trials between conditions. The advantage of this measure is that no explicit threshold needs to be assumed for classification. Another equivalent metric is the area under the receiver operating characteristic curve (AUC), which is related to d-prime for normally distributed classes by AUC = 0.5 + erf (d-prime/2)/2, where erf is the error function. Therefore, d-prime values of 0.1, 0.2 and 0.3 (which is about the maximum we obtained) correspond to AUC values of 0.52, 0.55 and 0.58. We used d-primes for discriminability due to their ease of computation and interpretation.

The d-prime metric is given by the formula:

$$\mathrm{d-prime} = \frac{\mu_1 - \mu_2}{\sqrt{\frac{(n_1 - 1)\sigma_1^2 + (n_2 - 1)\sigma_2^2}{n_1 + n_2 - 2}}}$$

where, μ_1 = mean across trials of attend/target-in or hit condition

μ_2 = mean across trials of attend/target-out or miss condition

σ_1^2 = variance across trials of attend/target-in or hit condition

σ_2^2 = variance across trials of attend/target-out or miss condition

n_1 = number of trials in attend/target-in or hit condition

n_2 = number of trials in attend/target-out or miss condition

Discriminability of traditional frequency bands:

We compared the discriminability of the neural measures in the following standard frequency bands: alpha (8-12 Hz), gamma (40-80 Hz), high-gamma (120-200 Hz) and SSVEP (18-22 Hz) frequency. We chose SSVEP frequency over a band of frequency rather than a single-frequency point because of frequency smoothing caused by using five tapers. To obtain the power and PPC in each band we averaged them over the frequencies of their respective

bands. We excluded the harmonics of SSVEP frequency (multiples of 20) in the gamma and high-gamma band. However, for the binning method where the frequency resolution was 20 Hz, we excluded only 60 Hz. We computed the correlations of the frequency-averaged power.

We could not analyze the behavioral discriminability (hits vs miss) at the population level by combining the activity of all the electrodes like we did previously (Prakash et al., 2021) for attention discriminability using linear discriminant analysis (Fisher, 1936) because there were an insufficient number of miss trials. The invertibility of the covariance matrix (required to obtain the weight vector) is guaranteed when the sample size is greater than the dimension (Li et al., 2006). But in our dataset, the number of missed trials (~20 trials (samples) per session on average after matching the target onset times) was lesser than the number of electrodes (~30 electrodes (dimension) per session on an average). Although, this limitation can be overcome by regularization (Guo et al., 2007), it underestimates the discriminability (see supplementary fig. 2 of (Prakash et al., 2021)).

Reference

Banerjee S, Grover S, Ganesh S, Sridharan D. 2019. Sensory and decisional components of endogenous attention are dissociable. *Journal of Neurophysiology* **122**:1538–1554. doi:10.1152/jn.00257.2019

Bastos AM, Vezoli J, Bosman CA, Schoffelen J-M, Oostenveld R, Dowdall JR, De Weerd P, Kennedy H, Fries P. 2015. Visual Areas Exert Feedforward and Feedback Influences through Distinct Frequency Channels. *Neuron* **85**:390–401. doi:10.1016/j.neuron.2014.12.018

Bokil H, Andrews P, Kulkarni JE, Mehta S, Mitra PP. 2010. Chronux: A platform for analyzing neural signals. *Journal of Neuroscience Methods* **192**:146–151. doi:10.1016/j.jneumeth.2010.06.020

Bosman CA, Schoffelen J-M, Brunet N, Oostenveld R, Bastos AM, Womelsdorf T, Rubehn B, Stieglitz T, De Weerd P, Fries P. 2012. Attentional Stimulus Selection through Selective Synchronization between Monkey Visual Areas. *Neuron* **75**:875–888. doi:10.1016/j.neuron.2012.06.037

Brookshire G. 2022. Putative rhythms in attentional switching can be explained by aperiodic temporal structure. *Nat Hum Behav* **6**:1280–1291. doi:10.1038/s41562-022-01364-0

Buffalo EA, Fries P, Landman R, Buschman TJ, Desimone R. 2011. Laminar differences in gamma and alpha coherence in the ventral stream. *Proceedings of the National Academy of Sciences* **108**:11262–11267. doi:10.1073/pnas.1011284108

Busch NA, Dubois J, VanRullen R. 2009. The Phase of Ongoing EEG Oscillations Predicts Visual Perception. *Journal of Neuroscience* **29**:7869–7876. doi:10.1523/JNEUROSCI.0113-09.2009

Busch NA, VanRullen R. 2010. Spontaneous EEG oscillations reveal periodic sampling of visual attention. *Proceedings of the National Academy of Sciences* **107**:16048–16053. doi:10.1073/pnas.1004801107

Carrasco M. 2011. Visual attention: The past 25 years. *Vision Research*, Vision Research 50th Anniversary Issue: Part 2 **51**:1484–1525. doi:10.1016/j.visres.2011.04.012

Cohen MR, Maunsell JHR. 2011. When Attention Wanders: How Uncontrolled Fluctuations in Attention Affect Performance. *J Neurosci* **31**:15802–15806. doi:10.1523/JNEUROSCI.3063-11.2011

Cohen MR, Maunsell JHR. 2010. A Neuronal Population Measure of Attention Predicts Behavioral Performance on Individual Trials. *J Neurosci* **30**:15241–15253. doi:10.1523/JNEUROSCI.2171-10.2010

Cohen MR, Maunsell JHR. 2009. Attention improves performance primarily by reducing interneuronal correlations. *Nat Neurosci* **12**:1594–1600. doi:10.1038/nn.2439

De Sousa C, Gaillard C, Di Bello F, Ben Hadj Hassen S, Ben Hamed S. 2021. Behavioral validation of novel high resolution attention decoding method from multi-units & local field potentials. *NeuroImage* **231**:117853. doi:10.1016/j.neuroimage.2021.117853

De Valois RL, Albrecht DG, Thorell LG. 1982. Spatial frequency selectivity of cells in macaque visual cortex. *Vision Research* **22**:545–559. doi:10.1016/0042-6989(82)90113-4

Esghaei M, Daliri MR. 2014. Decoding of Visual Attention from LFP Signals of Macaque MT. *PLOS ONE* **9**:e100381. doi:10.1371/journal.pone.0100381

Ferro D, Van Kempen J, Boyd M, Panzeri S, Thiele A. 2021. Directed information exchange between cortical layers in macaque V1 and V4 and its modulation by selective attention. *Proc Natl Acad Sci USA* **118**:e2022097118. doi:10.1073/pnas.2022097118

Fiebelkorn IC, Pinsk MA, Kastner S. 2018. A Dynamic Interplay within the Frontoparietal Network Underlies Rhythmic Spatial Attention. *Neuron* **99**:842-853.e8. doi:10.1016/j.neuron.2018.07.038

Fisher RA. 1936. The Use of Multiple Measurements in Taxonomic Problems. *Annals of Eugenics* **7**:179–188. doi:10.1111/j.1469-1809.1936.tb02137.x

Fries P. 2015. Rhythms for Cognition: Communication through Coherence. *Neuron* **88**:220–235. doi:10.1016/j.neuron.2015.09.034

Fries P, Reynolds JH, Rorie AE, Desimone R. 2001. Modulation of Oscillatory Neuronal Synchronization by Selective Visual Attention. *Science* **291**:1560–1563.

Ghosh S, Maunsell JHR. 2021. Single trial neuronal activity dynamics of attentional intensity in monkey visual area V4. *Nat Commun* **12**:2003. doi:10.1038/s41467-021-22281-2

Gregoriou GG, Gotts SJ, Zhou H, Desimone R. 2009. High-Frequency, Long-Range Coupling Between Prefrontal and Visual Cortex During Attention. *Science* **324**:1207–1210. doi:10.1126/science.1171402

Guo Y, Hastie T, Tibshirani R. 2007. Regularized linear discriminant analysis and its application in microarrays. *Biostatistics* **8**:86–100. doi:10.1093/biostatistics/kxj035

Hafed ZM, Krauzlis RJ. 2012. Similarity of superior colliculus involvement in microsaccade and saccade generation. *J Neurophysiol* **107**:1904–1916. doi:10.1152/jn.01125.2011

Hanslmayr S, Aslan A, Staudigl T, Klimesch W, Herrmann CS, Bäuml K-H. 2007. Prestimulus oscillations predict visual perception performance between and within subjects. *NeuroImage* **37**:1465–1473. doi:10.1016/j.neuroimage.2007.07.011

Harris AM, Dux PE, Mattingley JB. 2018. Detecting Unattended Stimuli Depends on the Phase of Prestimulus Neural Oscillations. *J Neurosci* **38**:3092–3101. doi:10.1523/JNEUROSCI.3006-17.2018

Hong L, Walz JM, Sajda P. 2014. Your Eyes Give You Away: Prestimulus Changes in Pupil Diameter Correlate with Poststimulus Task-Related EEG Dynamics. *PLOS ONE* **9**:e91321. doi:10.1371/journal.pone.0091321

Hwang EJ, Andersen RA. 2013. The utility of multichannel local field potentials for brain–machine interfaces. *J Neural Eng* **10**:046005. doi:10.1088/1741-2560/10/4/046005

Iemi L, Chaumon M, Crouzet SM, Busch NA. 2017. Spontaneous Neural Oscillations Bias Perception by Modulating Baseline Excitability. *J Neurosci* **37**:807–819. doi:10.1523/JNEUROSCI.1432-16.2016

Jarvis MR, Mitra PP. 2001. Sampling Properties of the Spectrum and Coherency of Sequences of Action Potentials. *Neural Computation* **13**:717–749. doi:10.1162/089976601300014312

Johnston R, Snyder AC, Schibler RS, Smith MA. 2022. EEG Signals Index a Global Signature of Arousal Embedded in Neuronal Population Recordings. *eNeuro* **9**. doi:10.1523/ENEURO.0012-22.2022

Kanth ST, Ray S. 2020. Electrocorticogram (ECoG) Is Highly Informative in Primate Visual Cortex. *J Neurosci* **40**:2430–2444. doi:10.1523/JNEUROSCI.1368-19.2020

Khayat PS, Niebergall R, Martinez-Trujillo JC. 2010. Frequency-Dependent Attentional Modulation of Local Field Potential Signals in Macaque Area MT. *J Neurosci* **30**:7037–7048. doi:10.1523/JNEUROSCI.0404-10.2010

Landau AN, Fries P. 2012. Attention Samples Stimuli Rhythmically. *Current Biology* **22**:1000–1004. doi:10.1016/j.cub.2012.03.054

Li T, Zhu S, Ogihara M. 2006. Using discriminant analysis for multi-class classification: an experimental investigation. *Knowl Inf Syst* **10**:453–472. doi:10.1007/s10115-006-0013-y

Limbach K, Corballis PM. 2016. Prestimulus alpha power influences response criterion in a detection task. *Psychophysiology* **53**:1154–1164. doi:10.1111/psyp.12666

Luo TZ, Maunsell JHR. 2019. Attention can be subdivided into neurobiological components corresponding to distinct behavioral effects. *Proceedings of the National Academy of Sciences* **116**:26187–26194. doi:10.1073/pnas.1902286116

Mayo JP, Maunsell JHR. 2016. Graded Neuronal Modulations Related to Visual Spatial Attention. *J Neurosci* **36**:5353–5361. doi:10.1523/JNEUROSCI.0192-16.2016

McAdams CJ, Maunsell JHR. 1999. Effects of Attention on Orientation-Tuning Functions of Single Neurons in Macaque Cortical Area V4. *J Neurosci* **19**:431–441. doi:10.1523/JNEUROSCI.19-01-00431.1999

Mitchell JF, Sundberg KA, Reynolds JH. 2009. Spatial Attention Decorrelates Intrinsic Activity Fluctuations in Macaque Area V4. *Neuron* **63**:879–888. doi:10.1016/j.neuron.2009.09.013

Motter BC. 1993. Focal attention produces spatially selective processing in visual cortical areas V1, V2, and V4 in the presence of competing stimuli. *Journal of Neurophysiology* **70**:909–919. doi:10.1152/jn.1993.70.3.909

Ni J, Wunderle T, Lewis CM, Desimone R, Diester I, Fries P. 2016. Gamma-Rhythmic Gain Modulation. *Neuron* **92**:240–251. doi:10.1016/j.neuron.2016.09.003

Podvalny E, King LE, He BJ. 2021. Spectral signature and behavioral consequence of spontaneous shifts of pupil-linked arousal in human. *eLife* **10**:e68265. doi:10.7554/eLife.68265

Prakash SS, Das A, Kanth ST, Mayo JP, Ray S. 2021. Decoding of Attentional State Using High-Frequency Local Field Potential Is As Accurate As Using Spikes. *Cerebral Cortex* **31**:4314–4328. doi:10.1093/cercor/bhab088

Prakash SS, Mayo JP, Ray S. 2022. Decoding of attentional state using local field potentials. *Current Opinion in Neurobiology* **76**:102589. doi:10.1016/j.conb.2022.102589

Ray S. 2022. Spike–Gamma Phase Relationship in the Visual Cortex. *Annual Review of Vision Science* **8**:361–381. doi:10.1146/annurev-vision-100419-104530

Ray S, Crone NE, Niebur E, Franaszczuk PJ, Hsiao SS. 2008. Neural Correlates of High-Gamma Oscillations (60–200 Hz) in Macaque Local Field Potentials and Their Potential Implications in Electrocorticography. *J Neurosci* **28**:11526–11536. doi:10.1523/JNEUROSCI.2848-08.2008

Ray S, Maunsell JHR. 2011. Different Origins of Gamma Rhythm and High-Gamma Activity in Macaque Visual Cortex. *PLOS Biology* **9**:e1000610. doi:10.1371/journal.pbio.1000610

Rohenkohl G, Bosman CA, Fries P. 2018. Gamma Synchronization between V1 and V4 Improves Behavioral Performance. *Neuron* **100**:953-963.e3. doi:10.1016/j.neuron.2018.09.019

Rotermund D, Ernst UA, Mandon S, Taylor K, Smiyukha Y, Kreiter AK, Pawelzik KR. 2013. Toward High Performance, Weakly Invasive Brain Computer Interfaces Using Selective Visual Attention. *J Neurosci* **33**:6001–6011. doi:10.1523/JNEUROSCI.4225-12.2013

Roy NA, Bak JH, Akrami A, Brody CD, Pillow JW. 2021. Extracting the dynamics of behavior in sensory decision-making experiments. *Neuron* **109**:597-610.e6. doi:10.1016/j.neuron.2020.12.004

Samaha J, Iemi L, Haegens S, Busch NA. 2020. Spontaneous Brain Oscillations and Perceptual Decision-Making. *Trends in Cognitive Sciences* **24**:639–653. doi:10.1016/j.tics.2020.05.004

Schneider M, Broggini AC, Dann B, Tzanou A, Uran C, Sheshadri S, Scherberger H, Vinck M. 2021. A mechanism for inter-areal coherence through communication based on connectivity and oscillatory power. *Neuron* **109**:4050-4067.e12. doi:10.1016/j.neuron.2021.09.037

Spyropoulos G, Schneider M, Kempen J van, Gieselmann MA, Thiele A, Vinck M. 2023. Distinct feedforward and feedback pathways for cell-type specific attention effects. doi:10.1101/2022.11.04.515185

Sridharan D, Steinmetz NA, Moore T, Knudsen EI. 2014. Distinguishing bias from sensitivity effects in multialternative detection tasks. *J Vis* **14**:16. doi:10.1167/14.9.16

Steinmetz NA, Moore T. 2014. Eye Movement Preparation Modulates Neuronal Responses in Area V4 When Dissociated from Attentional Demands. *Neuron* **83**:496–506. doi:10.1016/j.neuron.2014.06.014

Thut G, Nietzel A, Brandt SA, Pascual-Leone A. 2006. α-Band Electroencephalographic Activity over Occipital Cortex Indexes Visuospatial Attention Bias and Predicts Visual Target Detection. *J Neurosci* **26**:9494–9502. doi:10.1523/JNEUROSCI.0875-06.2006

Tremblay S, Doucet G, Pieper F, Sachs A, Martinez-Trujillo J. 2015. Single-Trial Decoding of Visual Attention from Local Field Potentials in the Primate Lateral Prefrontal Cortex Is Frequency-Dependent. *J Neurosci* **35**:9038–9049. doi:10.1523/JNEUROSCI.1041-15.2015

van Kempen J, Loughnane GM, Newman DP, Kelly SP, Thiele A, O'Connell RG, Bellgrove MA. 2019. Behavioural and neural signatures of perceptual decision-making are modulated by pupil-linked arousal. *eLife* **8**:e42541. doi:10.7554/eLife.42541

van Kerkoerle T, Self MW, Dagnino B, Gariel-Mathis M-A, Poort J, van der Togt C, Roelfsema PR. 2014. Alpha and gamma oscillations characterize feedback and feedforward processing in monkey visual cortex. *Proceedings of the National Academy of Sciences* **111**:14332–14341. doi:10.1073/pnas.1402773111

Vinck M, van Wingerden M, Womelsdorf T, Fries P, Pennartz CMA. 2010. The pairwise phase consistency: A bias-free measure of rhythmic neuronal synchronization. *NeuroImage* **51**:112–122. doi:10.1016/j.neuroimage.2010.01.073

Willett SM, Mayo JP. 2023. Microsaccades are directed toward the midpoint between targets in a variably cued attention task. *Proceedings of the National Academy of Sciences* **120**:e2220552120. doi:10.1073/pnas.2220552120

Womelsdorf T, Fries P, Mitra PP, Desimone R. 2006. Gamma-band synchronization in visual cortex predicts speed of change detection. *Nature* **439**:733–736. doi:10.1038/nature04258

Zhou YJ, Iemi L, Schoffelen J-M, Lange FP de, Haegens S. 2021. Alpha Oscillations Shape Sensory Representation and Perceptual Sensitivity. *J Neurosci* **41**:9581–9592. doi:10.1523/JNEUROSCI.1114-21.2021

Figure legends

Figure 1: Comparison of firing rate (FR) and local field potential (LFP) power across validly cued attention and behavioral conditions for non-matched and matched target onset time distributions.

(A) Mean peri-stimulus time histogram (PSTH) relative to the target onset time for the conditions in which attention was validly cued into or outside the receptive field of a neuron and the subject either detected (hit) or missed the target, namely, Attend-In Valid Hit (AIVH; blue), Attend-Out Valid Hit (AOVH; red), Attend-in Valid Miss (AIVM; cyan) and Attend-Out Valid Miss (AOVM; magenta). Inset shows the mean firing rate over the same time period as PSTH for the four conditions. The mean is taken across 677 electrodes recorded across 22 sessions in two monkeys. Only sessions in which at least 10 stimulus repeats were available were used for analysis. Shaded lines and error bars (not visible for most traces) indicate the s.e.m across the 677 electrodes.

(B) Mean event-related potential (ERP) for the four conditions.

(C) Mean change in power spectral density in decibels for all the validly cued conditions relative to Attend-out Valid Hit (AOVH) condition.

(D) Mean change in LFP power spectral density in decibels between attend-in and attend-out conditions for hit (AIVH and AOVH; green) and miss (AIVM and AOVM; yellow) conditions. The horizontal dashed black line marks the zero of the y-axis.

(E) Mean change in power spectral density between hit and miss condition for Attend-In (AIVH and AIVM; blue) and Attend-Out (AOVH and AOVM; red) conditions. The horizontal dashed black line marks the zero of the y-axis.

(F) Mean d-prime (the ratio of the mean difference and pooled standard deviation of two conditions) of LFP power (solid lines) and firing rate (dashed color lines) between attend-in and attend-out conditions for hit (green) and miss (yellow) conditions. The horizontal dashed black line marks the zero of the y-axis.

(G) Mean d-prime of LFP power (solid lines) and firing rate (dashed color lines) between hit and miss condition for Attend-In (blue) and Attend-out (red) conditions. The horizontal dashed black line marks the zero of the y-axis.

(H) Frequency distribution of target onset time for the four validly cued conditions of all the sessions. The number in the brackets indicate total number of trials in the respective conditions.

(I) – (O) Same as (A)– (G) but for the case where the target onset time distributions of hit and miss conditions are matched separately for each attention condition (Attend-In and Attend-Out). Here the mean is first taken across 643 electrodes recorded across 21 sessions in two monkeys and then averaged across 50 bootstrap iterations of target onset time matched trials selection. Shaded lines and error bars indicate the bootstrap mean of s.e.m across the 643 electrodes.

(P) Mean d-prime of LFP power between attend-in and attend-out conditions for hit condition where LFP power is estimated by Multitaper method using time-frequency bandwidth product (TW) of 1 (darkest green), 3 (dark green), 5 (light green) and 10 (lightest green). The dashed green line indicates the d-prime of firing rate between the same conditions. The horizontal dashed black line marks the zero of the y-axis.

Figure 2: Comparison of LFP phase and pairwise phase consistency of individual electrodes and trial-wise firing rate correlation, LFP power correlation and pairwise phase consistency (PPC) of electrode pairs across validly cued attention and behavioral conditions

(A) Mean sine of the LFP phase angle for Attend-In Valid Hit (AIVH; blue), Attend-Out Valid Hit (AOVH; red), Attend-In Valid Miss (AIVM; cyan), Attend-Out Valid Miss (AOVM; magenta) conditions.

(B) Mean d-prime of firing rate (dashed color lines) and sine of the LFP phase angle (solid lines) between attend-in and attend-out conditions for hit (green) and miss (yellow) conditions. The horizontal dashed black line marks the zero of the y-axis.

(C) Mean d-prime of firing rate (dashed color lines) and sine of the LFP phase angle (solid lines) between hit and miss conditions for attend-in (blue) and attend-out (red) conditions. The horizontal dashed black line marks the zero of the y-axis.

(D) Mean single electrode pairwise phase consistency (PPC; see Methods for details) for the four conditions as in (A).

(E) Mean change in single electrode PPC between attend-in and attend-out conditions for hit (green) and miss condition (yellow). The horizontal dashed black line marks the zero of the y-axis.

(F) Mean change in single electrode PPC between hit and miss conditions for attend-in (blue) and attend-out condition (red). The horizontal dashed black line marks the zero of the y-axis. In (A) – (F) mean and s.e.m are computed like in Fig. 1I – 1O.

(G) Mean change in trial-wise firing rate correlations for the four conditions relative to Attend-Out Valid Hit (AOVH) condition. Dashed black line indicates the zero of y-axis.

(H) Mean change in trial-wise LFP correlations (solid lines) and firing rate correlation (dashed color lines) between attend-in condition and attend-out condition for hit (green) and miss trials (yellow). The dashed black line indicates the zero of y-axis.

(I) Mean change in trial-wise LFP correlation (solid lines) and firing rate correlation (dashed color lines) between hit condition and miss condition for validly cued attend-in (blue) and attend-out (red) conditions. The dashed black line indicates the zero of y-axis.

(J) Mean pairwise phase consistency (PPC) across trials for the four conditions as in (A).

(K-L) Same as (E-F) but for pairwise phase consistency (PPC) across trials.

In (G) – (L) Mean was taken across 50 bootstrap samples of mean across 5754 pairs and shaded lines and error bar indicate the bootstrap mean of s.e.m across 5754 electrode pairs.

Figure 3: Illustration of methods used for estimating correlation and pairwise phase consistency within a trial

Binning method (left panel): A single-trial LFP signal of 500 ms duration from two electrodes is first divided into 10 non-overlapping bins of 50 ms each. Then, the power and phase of each 50 ms LFP segments of the two electrodes were estimated by Fourier transform. Subsequently, we estimated the power correlation and pairwise phase consistency across the ten bins between the pair of electrodes at each frequency between 0- 200 Hz with 20 Hz resolution. Similarly, the spikes from the two electrodes were also binned and firing rate correlations between the two electrodes were computed across bins (lower left panel).

Multitaper method (right panel): We used an alternate method to obtain multiple estimate of power and phase using the Multitaper method. LFP signal of 500 ms duration of two electrodes were first multiplied by nine orthogonal Slepian tapers of same length, then power

and phase of these nine tapered LFP signals were obtained by Fourier transform. Power correlation and PPC were calculated between electrode pairs across tapers at frequencies between 0-200 Hz with 2Hz resolution. The black dot in the PPC vs frequency and correlation vs frequency plots indicate the frequency whose amplitude and phase are shown in the polar plot in top panel and whose power scatter plot is shown.

Figure 4: Comparison of single trial bin-wise firing rate correlation, bin-wise and taper-wise LFP power correlation and pairwise phase consistency (PPC) across validly cued attention and behavioral conditions

(A) Mean change in single trial bin-wise LFP power correlation (solid lines) and firing rate correlation (dashed color lines) between validly cued attend-in and attend-out conditions for hit (green) and miss (yellow) conditions. Single trial bin-wise correlation was measured by dividing the analysis period of 500 ms into 10 non-overlapping bins and measuring the firing rate or power correlation across bins. Since power was estimated for signals of 50 ms duration, the frequency resolution is 20 Hz. Dashed black line indicates the zero of y-axis.

(B) Mean d-prime of bin-wise LFP power correlation (solid lines) and firing rate correlation (dashed color lines) between validly cued attend-in and attend-out conditions for hit (green) and miss (yellow) conditions. Dashed black line indicates the zero of y-axis.

(C) Mean change in bin-wise LFP power correlation (solid lines) and firing rate correlation (dashed color lines) between hit and miss conditions for validly cued attend-in (blue) and attend-out (red) conditions. Dashed black line indicates the zero of y-axis.

(D) Mean d-prime of bin-wise LFP power correlation (solid lines) and firing rate correlation (dashed color lines) between hit and miss condition for validly cued attend-in (blue) and attend-out (red) conditions. Dashed black line indicates the zero of y-axis.

(E) – (H) Same as (A) – (D) but for single trial bin-wise PPC. Single trial bin-wise PPC was computed across the same 10 non-overlapping bins used to compute power correlations.

(I) – (P) Same as (A) – (H) but for single trial taper-wise power correlation and PPC. Here power correlation and PPC are computed by using multi-taper method. Specifically, we use TW=5 to get 9 (2TW-1) estimates of power and phase values per trial and compute the power correlation or PPC between electrode pairs across these nine values.

In (A) – (P) Mean was taken across 50 bootstrap samples of mean across 5754 pairs and shaded lines indicate the bootstrap mean of s.e.m across 5754 electrode pairs.

Figure 5: Summary plot comparing across the d-primes of all the measures for spikes, LFP power and phase in different frequency bands for validly cued attention and behavioral comparison.

(A) D-prime of firing rate/ LFP power (red), sine of the phase angle (blue), firing rate/ LFP power correlation across the bins (green), LFP power correlation across the tapers (magenta), pairwise phase consistency (PPC) across bins (brown), PPC across tapers (purple) for spikes, alpha (8-12 Hz), SSVEP (18-22 Hz), gamma (40-80 Hz) and high-gamma (120-200 Hz) power between attend-in and attend-out conditions for hit trials. Note that for spikes, only d-primes of firing rate and bin-wise correlation exist because rest of the measures cannot be computed for the spike data whereas for alpha-band, d-prime of bin-wise measures ($\text{Correlation}_{\text{Bin}}$ and PPC_{Bin}) are absent because the frequency resolution in the binning method was 20 Hz. '***' indicates p-value<0.001, '**' indicates 0.001<p-values<0.01, '*' indicates the 0.01<p-values<0.05 and no asterisks are shown for p-values>0.05. Negative d-prime values were converted to positive values by multiplying with -1 before performing the

significance test since we were comparing only the magnitude. All the p-values are Bonferroni corrected for multiple comparisons.

(B) Same as (A) but for the d-prime between the hit and miss conditions of Attend-in condition.

Supplementary figure 1: Comparison of firing rate (FR) and local field potential (LFP) power across neutrally cued attention and behavioral conditions for non-matched and matched target onset time distributions.

(A) Mean peri-stimulus time histogram (PSTH) relative to the target onset time for the neutrally cued conditions in which attention was cued to both visual hemifields simultaneously and target could appear at either of the location with 50% probability. Unlike the valid cue condition where the conditions were divided based on attention location, here the conditions are divided based on where the target eventually appeared, namely Target-In Neutral Hit (TINH; blue), Target-Out Neutral Hit (TONH; red), Target-In Neutral Miss (TINM; cyan), Target-Out Neutral Miss (TONM; magenta). Inset shows the mean firing rate over the same time period as PSTH for the four conditions. Mean is taken across 696 electrodes from 22 sessions in two monkeys. Shaded lines and error bars indicate the s.e.m across the 696 electrodes.

(B) Mean ERP for the four conditions described in A.

(C) Mean change in power spectral density for all the neutrally cued conditions relative to Target-Out Neutral Hit (TONH) condition.

(D) Mean change in LFP power spectral density in decibels between Target-In and Target-Out conditions for hit (TINH and TONH; green) and miss (TINM and TONM; yellow). The horizontal dashed black line marks the zero of the y-axis.

(E) Mean change in LFP power spectral density between hit and miss condition for neutrally cued Target-In (TINH and TINM; blue) and Target-Out (TONH and TONM; red) conditions. The horizontal dashed black line indicates the zero of the y-axis.

(F) Mean d-prime of LFP power (solid lines) and firing rate (dashed color lines) between neutrally cued attend-in and attend-out conditions for hit (green) and miss (yellow) conditions. The horizontal dashed black line marks the zero of the y-axis.

(G) Mean d-prime of LFP power (solid lines) and firing rate (dashed color lines) between hit and miss condition for neutrally cued Target-In (blue) and Target-out (red) conditions. The horizontal dashed black line indicates the zero of the y-axis.

(H) Frequency distribution of target onset time for the four neutrally cued conditions of all the sessions. The number in the brackets indicates total number of trials in the respective conditions.

(I) – (O) Same as (A) – (G) but for the case where the target onset time distributions of hit and miss conditions are matched separately for Target-In and Target-Out conditions. Here the mean is first taken across 659 electrodes recorded across 21 sessions in two monkeys and then averaged across 50 bootstrap iterations. Shaded lines and error bars indicate the bootstrap mean of s.e.m across the 659 electrodes.

(P) Mean d-prime of LFP power between Target-In and Target-Out conditions for hit condition where LFP power is estimated by Multitaper method using time-frequency bandwidth product (TW) of 1 (darkest green), 3 (dark green), 5 (light green) and 10 (lightest

green). The dashed green line indicates the d-prime of firing rate between the same conditions. The horizontal dashed black line marks the zero of the y-axis.

Supplementary figure 2: Comparison of LFP phase and pairwise phase consistency of individual electrodes and trial-wise firing rate correlation, LFP power correlation and pairwise phase consistency (PPC) of electrode pairs across neutrally cued attention and behavioral conditions

Same as figure 2 but for the neutrally cued conditions. In (A)–(F) mean and s.e.m are computed like in Supplementary figure 1I – 1O. In (G)-(L) mean was taken across 50 bootstrap samples of mean across 5985 pairs and shaded lines and error bar indicate the bootstrap mean of s.e.m across 5985 electrode pairs.

Supplementary figure 3: Comparison of single trial bin-wise firing rate correlation, bin-wise and taper-wise LFP power correlation and pairwise phase consistency (PPC) across neutrally cued attention and behavioral conditions

Same as figure 4 but for neutrally cued conditions. Mean and s.e.m were computed like in supplementary figure 2G – 2L.

Supplementary figure 4: Summary plot comparing across the d-primes of all the measures for spikes, LFP power and phase in different frequency bands for neutrally cued attention and behavioral comparison.

Same as figure 5 but for neutrally cued condition.

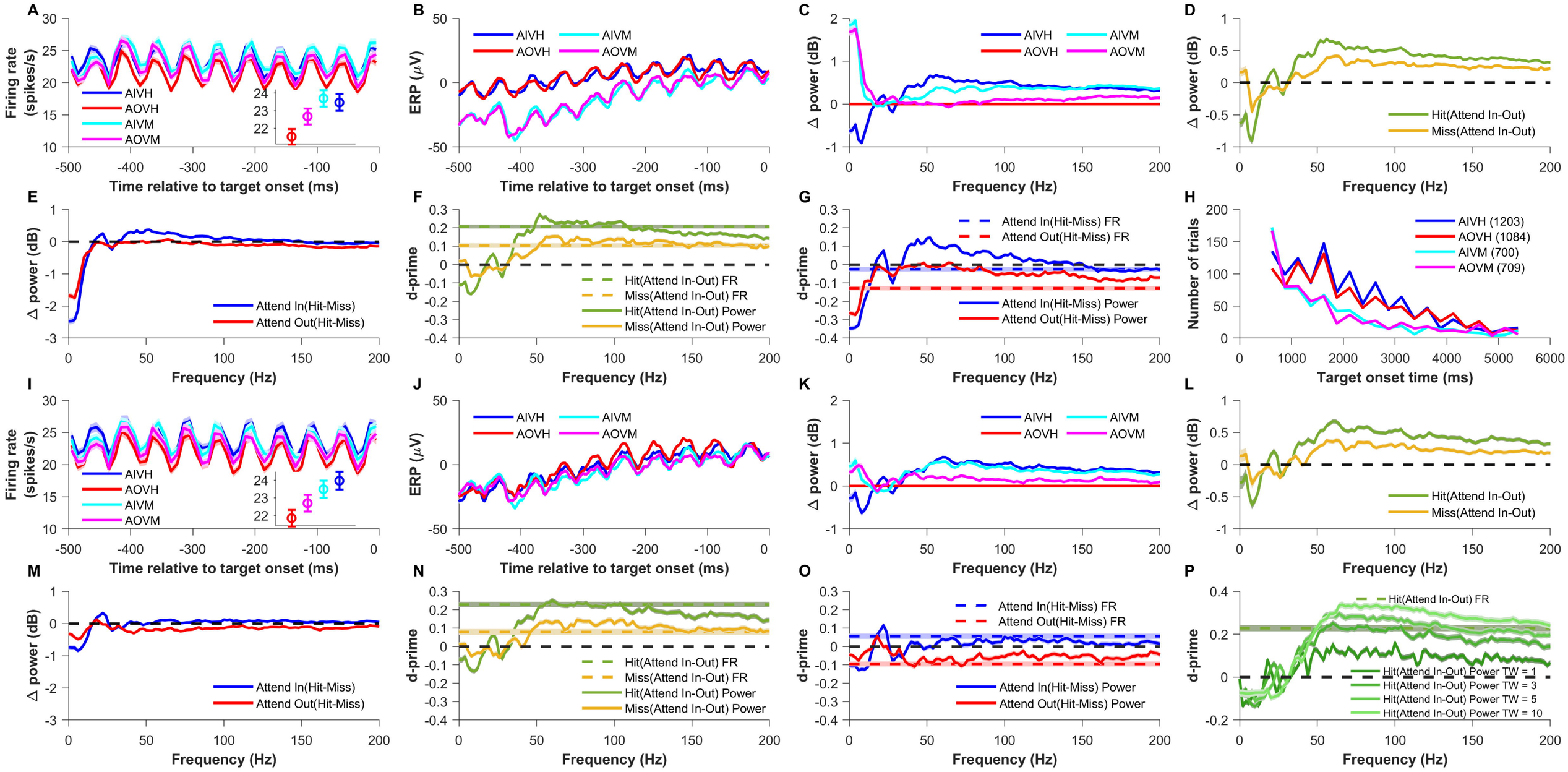
A
Firing rate (spikes/s)
AIVH
AOVH
AIVM
AOVM
Time relative to target onset (ms)
B
ERP (μV)
AIVH
AOVH
AIVM
AOVM
Time relative to target onset (ms)
C
Δ power (dB)
AIVH
AOVH
AIVM
AOVM
Frequency (Hz)
D
Δ power (dB)
Hit(Attend In-Out)
Miss(Attend In-Out)
Frequency (Hz)
E
Δ power (dB)
Attend In(Hit-Miss)
Attend Out(Hit-Miss)
Frequency (Hz)
F
d-prime
Hit(Attend In-Out) FR
Miss(Attend In-Out) FR
Hit(Attend In-Out) Power
Miss(Attend In-Out) Power
Frequency (Hz)
G
d-prime
Attend In(Hit-Miss) FR
Attend Out(Hit-Miss) FR
Attend In(Hit-Miss) Power
Attend Out(Hit-Miss) Power
Frequency (Hz)
H
Number of trials
AIVH (1203)
AOVH (1084)
AIVM (700)
AOVM (709)
Target onset time (ms)
I
Firing rate (spikes/s)
AIVH
AOVH
AIVM
AOVM
Time relative to target onset (ms)
J
ERP (μV)
AIVH
AOVH
AIVM
AOVM
Time relative to target onset (ms)
K
Δ power (dB)
AIVH
AOVH
AIVM
AOVM
Frequency (Hz)
L
Δ power (dB)
Hit(Attend In-Out)
Miss(Attend In-Out)
Frequency (Hz)
M
Δ power (dB)
Attend In(Hit-Miss)
Attend Out(Hit-Miss)
Frequency (Hz)
N
d-prime
Hit(Attend In-Out) FR
Miss(Attend In-Out) FR
Hit(Attend In-Out) Power
Miss(Attend In-Out) Power
Frequency (Hz)
O
d-prime
Attend In(Hit-Miss) FR
Attend Out(Hit-Miss) FR
Attend In(Hit-Miss) Power
Attend Out(Hit-Miss) Power
Frequency (Hz)
P
d-prime
Hit(Attend In-Out) FR
Hit(Attend In-Out) Power TW = 1
Hit(Attend In-Out) Power TW = 3
Hit(Attend In-Out) Power TW = 5
Hit(Attend In-Out) Power TW = 10
Frequency (Hz)

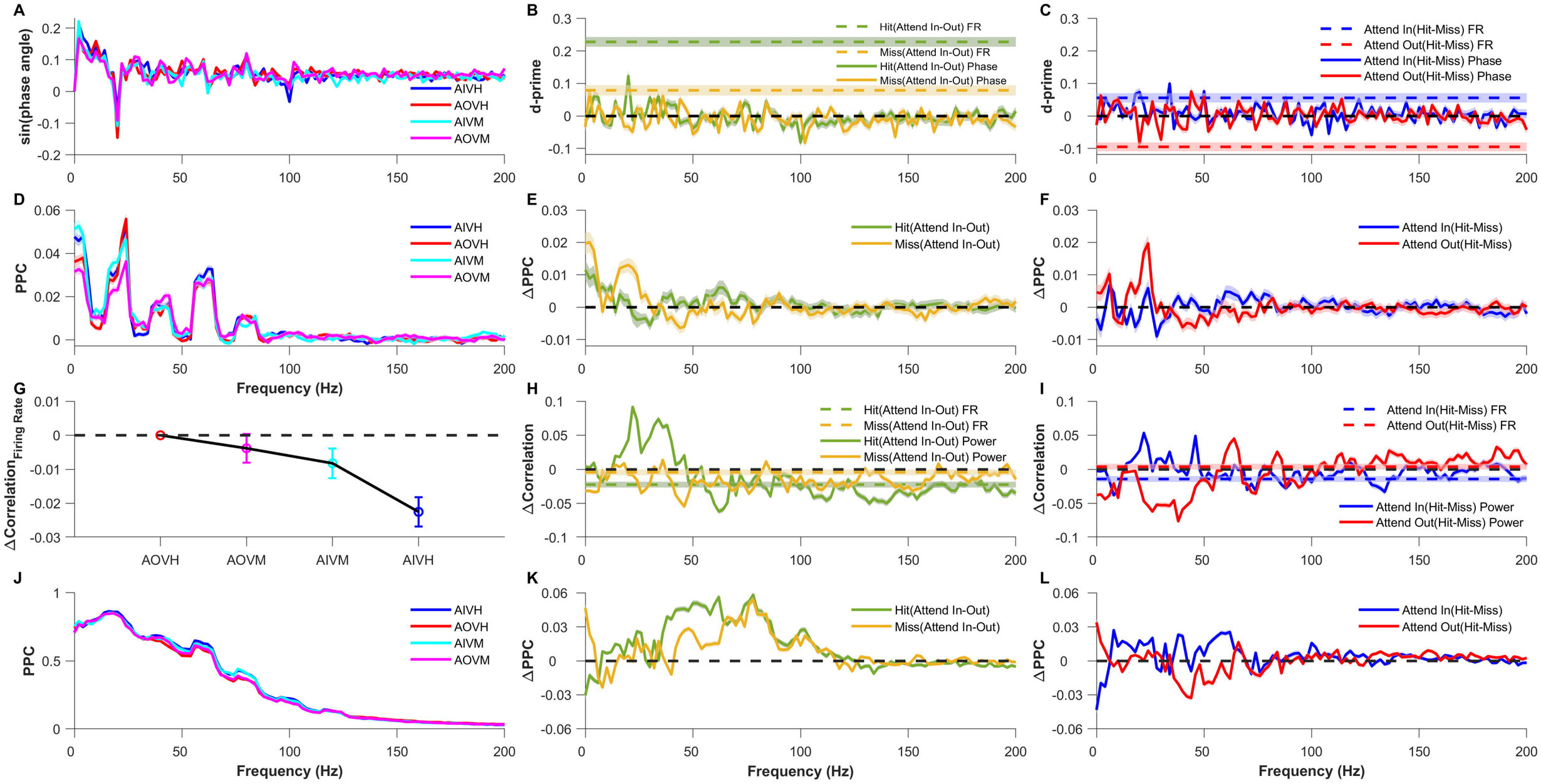
A
sin(phase angle)
AIVH
AOVH
AIVM
AOVM
B
d-prime
Hit(Attend In-Out) FR
Miss(Attend In-Out) FR
Hit(Attend In-Out) Phase
Miss(Attend In-Out) Phase
C
d-prime
Attend In(Hit-Miss) FR
Attend Out(Hit-Miss) FR
Attend In(Hit-Miss) Phase
Attend Out(Hit-Miss) Phase
D
PPC
AIVH
AOVH
AIVM
AOVM
Frequency (Hz)
E
ΔPPC
Hit(Attend In-Out)
Miss(Attend In-Out)
F
ΔPPC
Attend In(Hit-Miss)
Attend Out(Hit-Miss)
G
ΔCorrelation Firing Rate
AOVH
AOVM
AIVM
AIVH
H
ΔCorrelation
Hit(Attend In-Out) FR
Miss(Attend In-Out) FR
Hit(Attend In-Out) Power
Miss(Attend In-Out) Power
I
ΔCorrelation
Attend In(Hit-Miss) FR
Attend Out(Hit-Miss) FR
Attend In(Hit-Miss) Power
Attend Out(Hit-Miss) Power
J
PPC
AIVH
AOVH
AIVM
AOVM
Frequency (Hz)
K
ΔPPC
Hit(Attend In-Out)
Miss(Attend In-Out)
Frequency (Hz)
L
ΔPPC
Attend In(Hit-Miss)
Attend Out(Hit-Miss)
Frequency (Hz)

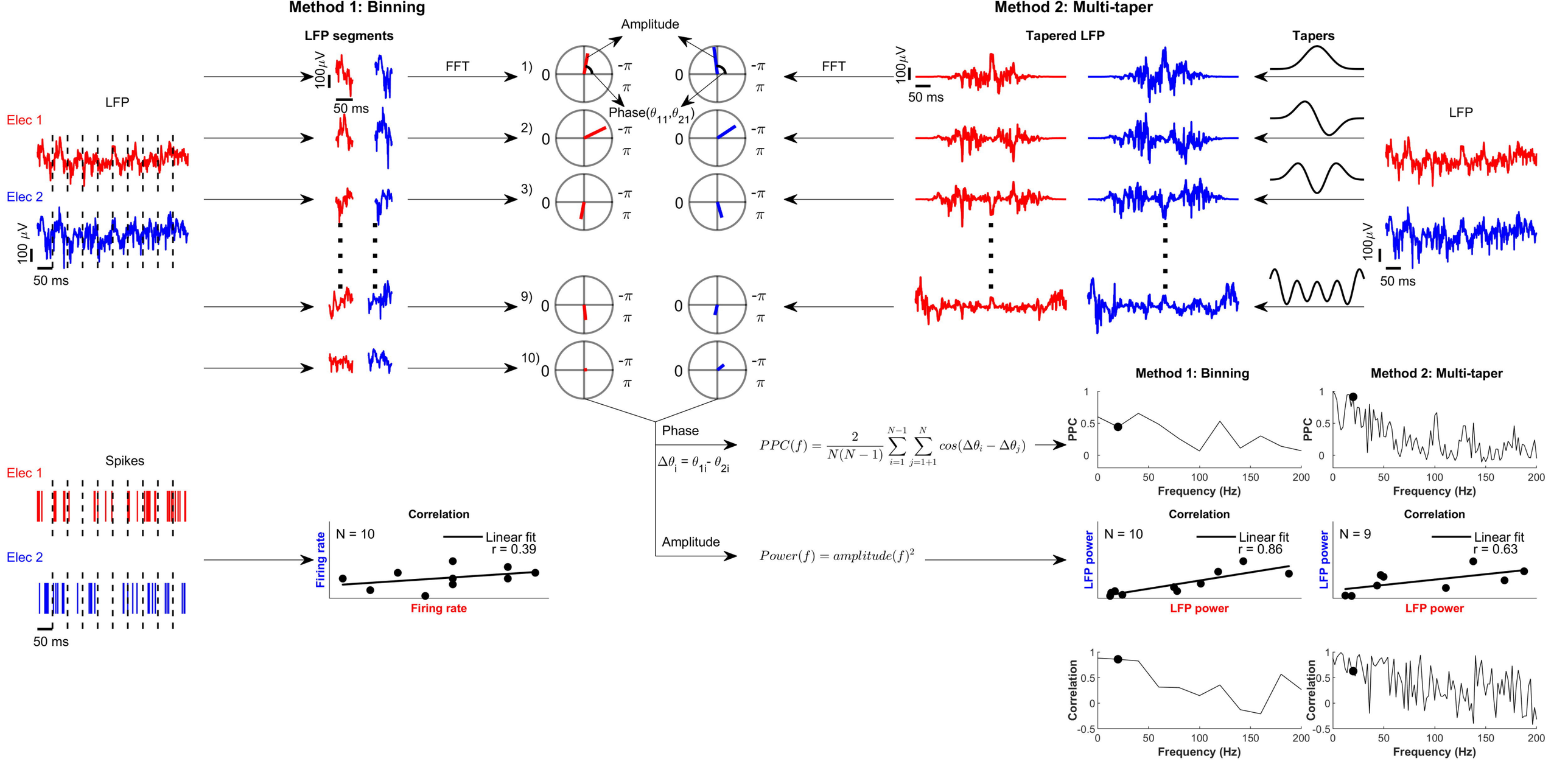
Method 1: Binning
Method 2: Multi-taper
LFP segments
Tapered LFP
Tapers
LFP
Elec 1
Elec 2
100 μV
50 ms
FFT
Amplitude
Phase(θ_{11},θ_{21})
1)
2)
3)
9)
10)
0
-π
π
Phase
$\Delta\theta_i = \theta_{1i} - \theta_{2i}$
Amplitude
$PPC(f) = \frac{2}{N(N-1)} \sum_{i=1}^{N-1} \sum_{j=1+1}^{N} cos(\Delta\theta_i - \Delta\theta_j)$
$Power(f) = amplitude(f)^2$
Spikes
Correlation
N = 10
Linear fit
r = 0.39
Firing rate
PPC
Frequency (Hz)
N = 10
r = 0.86
N = 9
r = 0.63
LFP power
Correlation

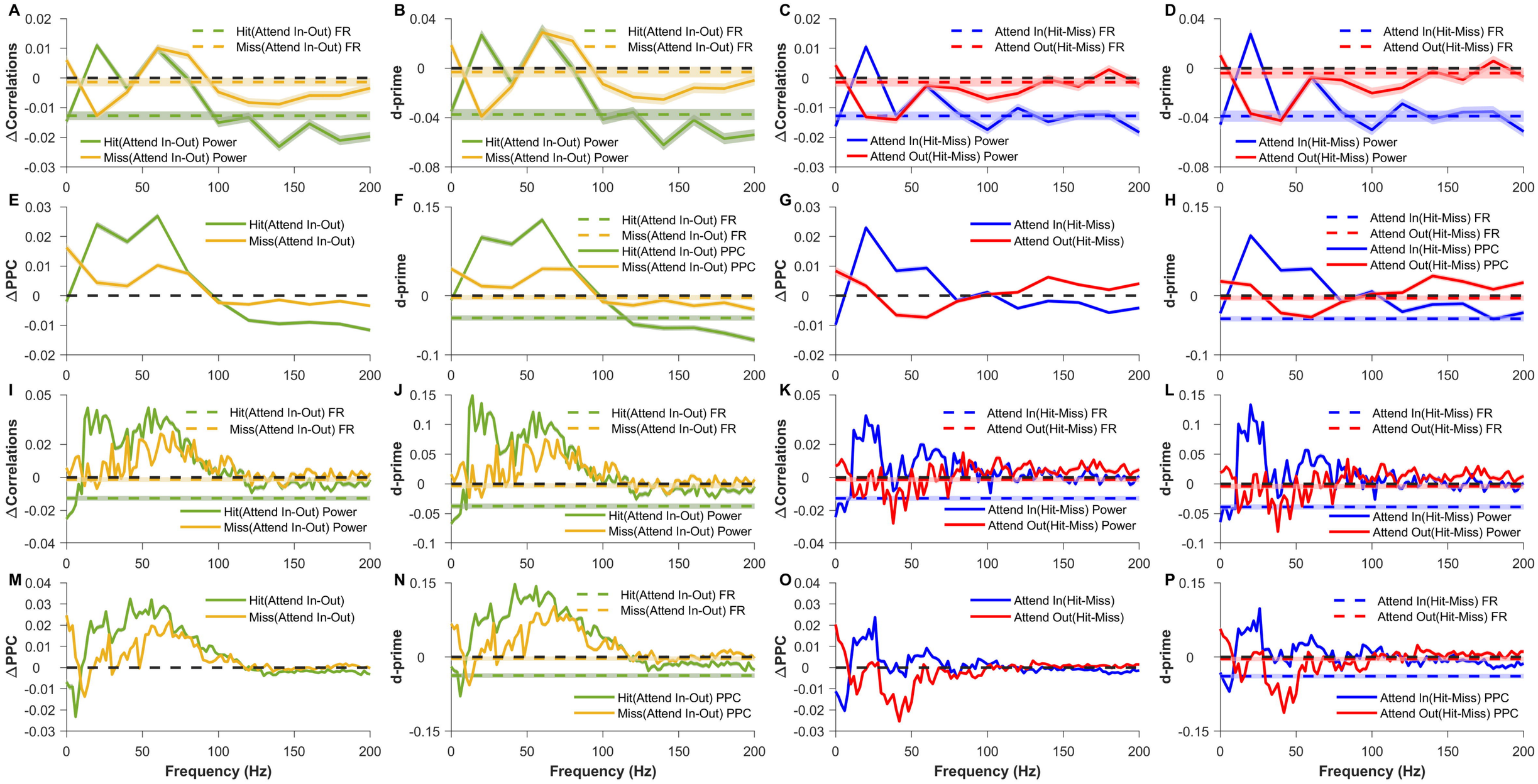
A
Hit(Attend In-Out) FR
Miss(Attend In-Out) FR
Hit(Attend In-Out) Power
Miss(Attend In-Out) Power
ΔCorrelations
B
Hit(Attend In-Out) FR
Miss(Attend In-Out) FR
Hit(Attend In-Out) Power
Miss(Attend In-Out) Power
d-prime
C
Attend In(Hit-Miss) FR
Attend Out(Hit-Miss) FR
Attend In(Hit-Miss) Power
Attend Out(Hit-Miss) Power
ΔCorrelations
D
Attend In(Hit-Miss) FR
Attend Out(Hit-Miss) FR
Attend In(Hit-Miss) Power
Attend Out(Hit-Miss) Power
d-prime
E
Hit(Attend In-Out)
Miss(Attend In-Out)
ΔPPC
F
Hit(Attend In-Out) FR
Miss(Attend In-Out) FR
Hit(Attend In-Out) PPC
Miss(Attend In-Out) PPC
d-prime
G
Attend In(Hit-Miss)
Attend Out(Hit-Miss)
ΔPPC
H
Attend In(Hit-Miss) FR
Attend Out(Hit-Miss) FR
Attend In(Hit-Miss) PPC
Attend Out(Hit-Miss) PPC
d-prime
I
Hit(Attend In-Out) FR
Miss(Attend In-Out) FR
Hit(Attend In-Out) Power
Miss(Attend In-Out) Power
ΔCorrelations
J
Hit(Attend In-Out) FR
Miss(Attend In-Out) FR
Hit(Attend In-Out) Power
Miss(Attend In-Out) Power
d-prime
K
Attend In(Hit-Miss) FR
Attend Out(Hit-Miss) FR
Attend In(Hit-Miss) Power
Attend Out(Hit-Miss) Power
ΔCorrelations
L
Attend In(Hit-Miss) FR
Attend Out(Hit-Miss) FR
Attend In(Hit-Miss) Power
Attend Out(Hit-Miss) Power
d-prime
M
Hit(Attend In-Out)
Miss(Attend In-Out)
ΔPPC
N
Hit(Attend In-Out) FR
Miss(Attend In-Out) FR
Hit(Attend In-Out) PPC
Miss(Attend In-Out) PPC
d-prime
O
Attend In(Hit-Miss)
Attend Out(Hit-Miss)
ΔPPC
P
Attend In(Hit-Miss) FR
Attend Out(Hit-Miss) FR
Attend In(Hit-Miss) PPC
Attend Out(Hit-Miss) PPC
d-prime
Frequency (Hz)
Frequency (Hz)
Frequency (Hz)
Frequency (Hz)

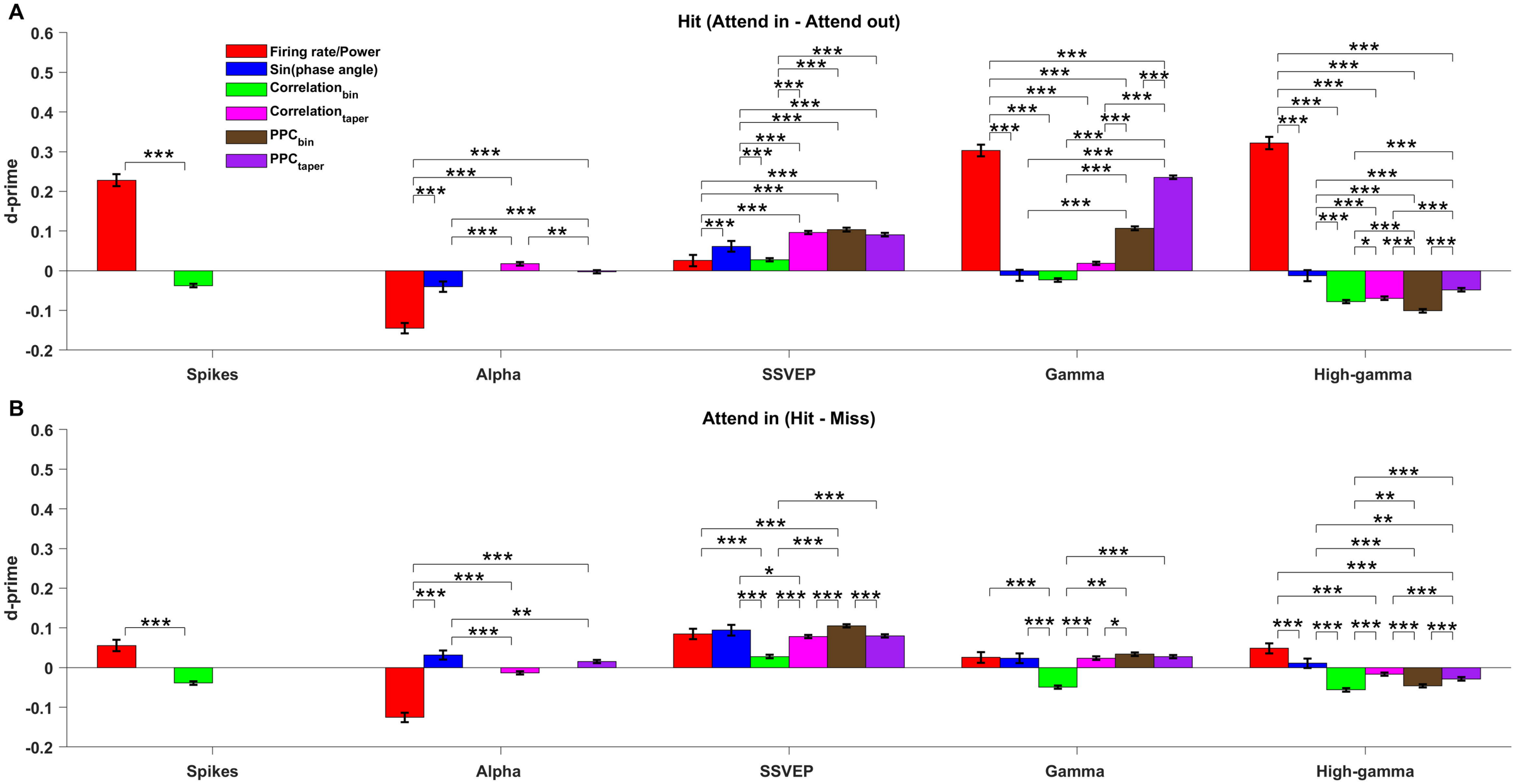
A
Hit (Attend in - Attend out)
Firing rate/Power
Sin(phase angle)
Correlation bin
Correlation taper
PPC bin
PPC taper
d-prime
0.6
0.5
0.4
0.3
0.2
0.1
0
-0.1
-0.2
Spikes
Alpha
SSVEP
Gamma
High-gamma
B
Attend in (Hit - Miss)
d-prime
0.6
0.5
0.4
0.3
0.2
0.1
0
-0.1
-0.2
Spikes
Alpha
SSVEP
Gamma
High-gamma

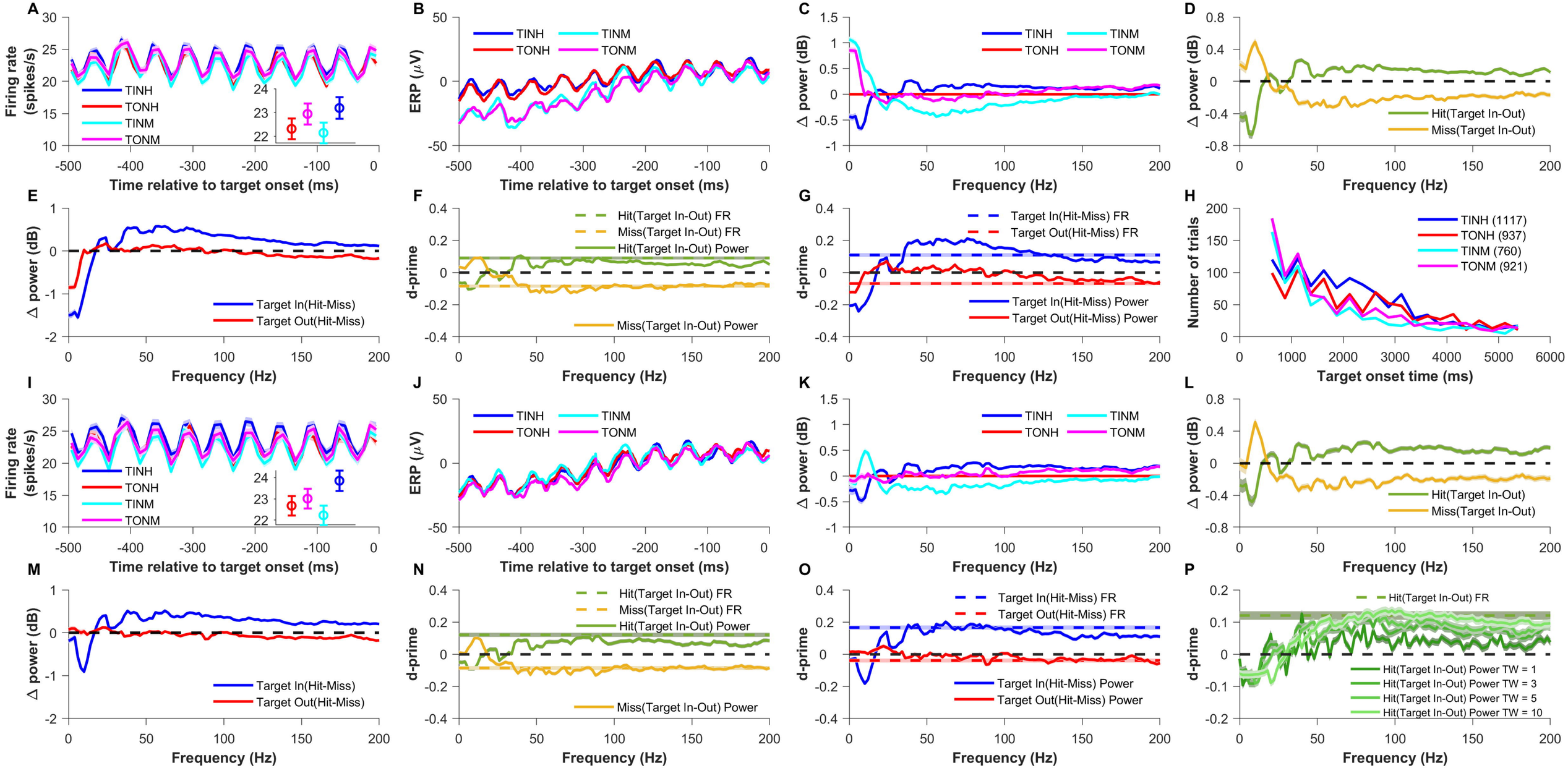
A
Firing rate (spikes/s)
TINH
TONH
TINM
TONM
Time relative to target onset (ms)
B
ERP (μV)
TINH
TONH
TINM
TONM
Time relative to target onset (ms)
C
Δ power (dB)
TINH
TONH
TINM
TONM
Frequency (Hz)
D
Δ power (dB)
Hit(Target In-Out)
Miss(Target In-Out)
Frequency (Hz)
E
Δ power (dB)
Target In(Hit-Miss)
Target Out(Hit-Miss)
Frequency (Hz)
F
d-prime
Hit(Target In-Out) FR
Miss(Target In-Out) FR
Hit(Target In-Out) Power
Miss(Target In-Out) Power
Frequency (Hz)
G
d-prime
Target In(Hit-Miss) FR
Target Out(Hit-Miss) FR
Target In(Hit-Miss) Power
Target Out(Hit-Miss) Power
Frequency (Hz)
H
Number of trials
TINH (1117)
TONH (937)
TINM (760)
TONM (921)
Target onset time (ms)
I
Firing rate (spikes/s)
TINH
TONH
TINM
TONM
Time relative to target onset (ms)
J
ERP (μV)
TINH
TONH
TINM
TONM
Time relative to target onset (ms)
K
Δ power (dB)
TINH
TONH
TINM
TONM
Frequency (Hz)
L
Δ power (dB)
Hit(Target In-Out)
Miss(Target In-Out)
Frequency (Hz)
M
Δ power (dB)
Target In(Hit-Miss)
Target Out(Hit-Miss)
Frequency (Hz)
N
d-prime
Hit(Target In-Out) FR
Miss(Target In-Out) FR
Hit(Target In-Out) Power
Miss(Target In-Out) Power
Frequency (Hz)
O
d-prime
Target In(Hit-Miss) FR
Target Out(Hit-Miss) FR
Target In(Hit-Miss) Power
Target Out(Hit-Miss) Power
Frequency (Hz)
P
d-prime
Hit(Target In-Out) FR
Hit(Target In-Out) Power TW = 1
Hit(Target In-Out) Power TW = 3
Hit(Target In-Out) Power TW = 5
Hit(Target In-Out) Power TW = 10
Frequency (Hz)

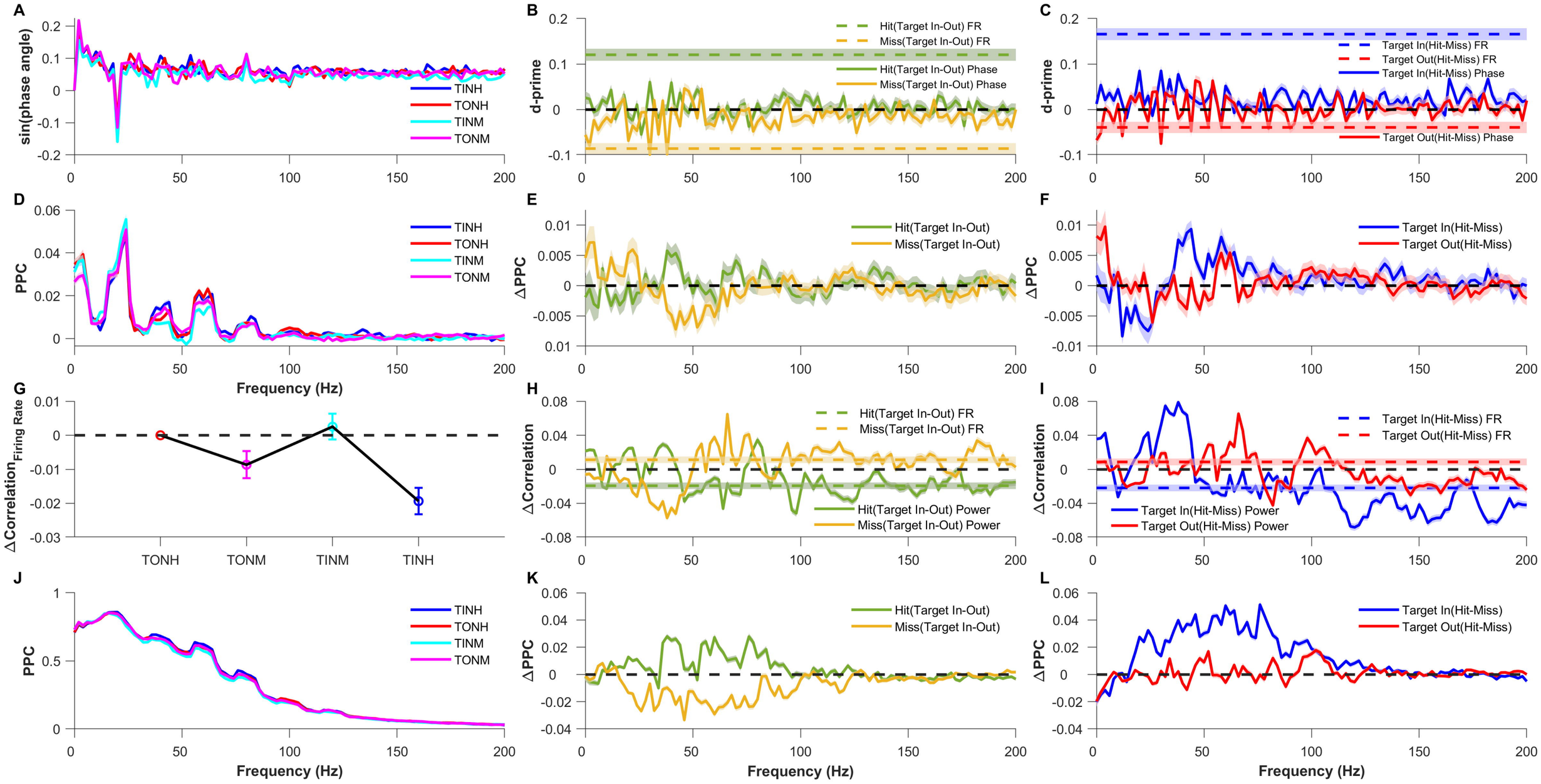
A
sin(phase angle)
TINH
TONH
TINM
TONM
B
d-prime
Hit(Target In-Out) FR
Miss(Target In-Out) FR
Hit(Target In-Out) Phase
Miss(Target In-Out) Phase
C
d-prime
Target In(Hit-Miss) FR
Target Out(Hit-Miss) FR
Target In(Hit-Miss) Phase
Target Out(Hit-Miss) Phase
D
PPC
TINH
TONH
TINM
TONM
Frequency (Hz)
E
ΔPPC
Hit(Target In-Out)
Miss(Target In-Out)
F
ΔPPC
Target In(Hit-Miss)
Target Out(Hit-Miss)
G
ΔCorrelation Firing Rate
TONH
TONM
TINM
TINH
H
ΔCorrelation
Hit(Target In-Out) FR
Miss(Target In-Out) FR
Hit(Target In-Out) Power
Miss(Target In-Out) Power
I
ΔCorrelation
Target In(Hit-Miss) FR
Target Out(Hit-Miss) FR
Target In(Hit-Miss) Power
Target Out(Hit-Miss) Power
J
PPC
TINH
TONH
TINM
TONM
Frequency (Hz)
K
ΔPPC
Hit(Target In-Out)
Miss(Target In-Out)
Frequency (Hz)
L
ΔPPC
Target In(Hit-Miss)
Target Out(Hit-Miss)
Frequency (Hz)

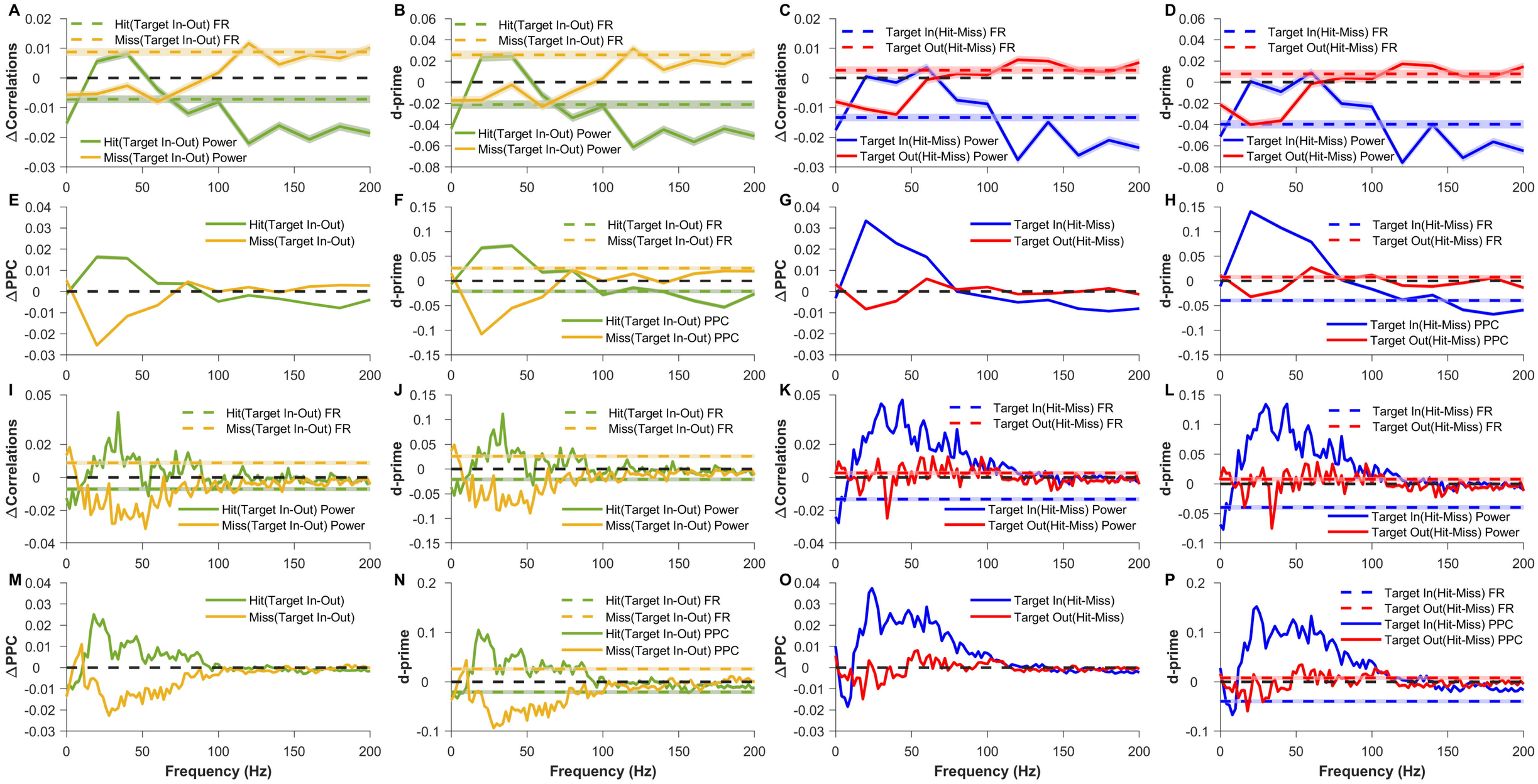
A
Hit(Target In-Out) FR
Miss(Target In-Out) FR
Hit(Target In-Out) Power
Miss(Target In-Out) Power
ΔCorrelations
B
Hit(Target In-Out) FR
Miss(Target In-Out) FR
Hit(Target In-Out) Power
Miss(Target In-Out) Power
d-prime
C
Target In(Hit-Miss) FR
Target Out(Hit-Miss) FR
Target In(Hit-Miss) Power
Target Out(Hit-Miss) Power
ΔCorrelations
D
Target In(Hit-Miss) FR
Target Out(Hit-Miss) FR
Target In(Hit-Miss) Power
Target Out(Hit-Miss) Power
d-prime
E
Hit(Target In-Out)
Miss(Target In-Out)
ΔPPC
F
Hit(Target In-Out) FR
Miss(Target In-Out) FR
Hit(Target In-Out) PPC
Miss(Target In-Out) PPC
d-prime
G
Target In(Hit-Miss)
Target Out(Hit-Miss)
ΔPPC
H
Target In(Hit-Miss) FR
Target Out(Hit-Miss) FR
Target In(Hit-Miss) PPC
Target Out(Hit-Miss) PPC
d-prime
I
Hit(Target In-Out) FR
Miss(Target In-Out) FR
Hit(Target In-Out) Power
Miss(Target In-Out) Power
ΔCorrelations
J
Hit(Target In-Out) FR
Miss(Target In-Out) FR
Hit(Target In-Out) Power
Miss(Target In-Out) Power
d-prime
K
Target In(Hit-Miss) FR
Target Out(Hit-Miss) FR
Target In(Hit-Miss) Power
Target Out(Hit-Miss) Power
ΔCorrelations
L
Target In(Hit-Miss) FR
Target Out(Hit-Miss) FR
Target In(Hit-Miss) Power
Target Out(Hit-Miss) Power
d-prime
M
Hit(Target In-Out)
Miss(Target In-Out)
ΔPPC
N
Hit(Target In-Out) FR
Miss(Target In-Out) FR
Hit(Target In-Out) PPC
Miss(Target In-Out) PPC
d-prime
O
Target In(Hit-Miss)
Target Out(Hit-Miss)
ΔPPC
P
Target In(Hit-Miss) FR
Target Out(Hit-Miss) FR
Target In(Hit-Miss) PPC
Target Out(Hit-Miss) PPC
d-prime
Frequency (Hz)
Frequency (Hz)
Frequency (Hz)
Frequency (Hz)

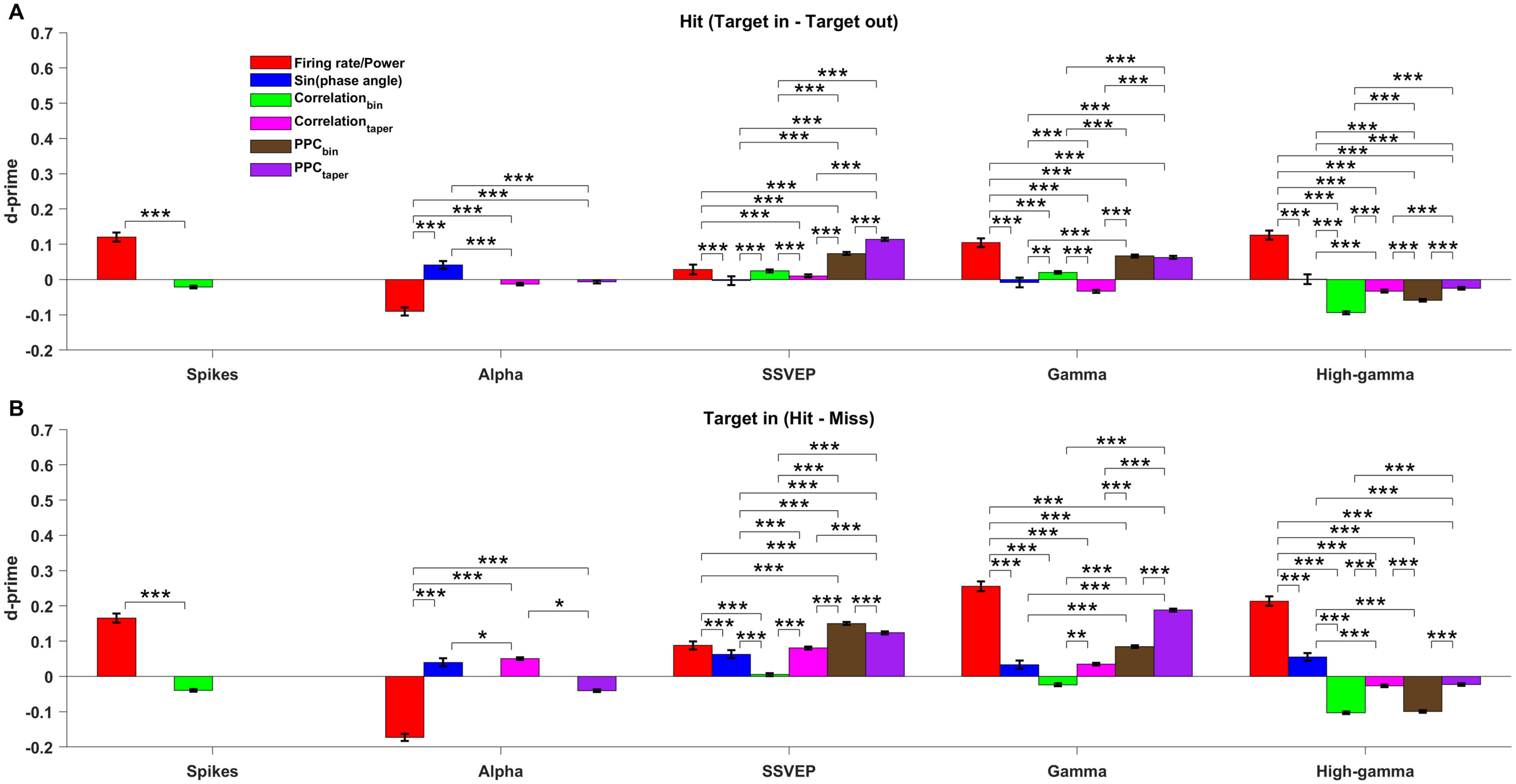
A
Hit (Target in - Target out)
Firing rate/Power
Sin(phase angle)
Correlation bin
Correlation taper
PPC bin
PPC taper
d-prime
0.7
0.6
0.5
0.4
0.3
0.2
0.1
0
-0.1
-0.2
Spikes
Alpha
SSVEP
Gamma
High-gamma
B
Target in (Hit - Miss)
d-prime
0.7
0.6
0.5
0.4
0.3
0.2
0.1
0
-0.1
-0.2
Spikes
Alpha
SSVEP
Gamma
High-gamma